

1 **B7-H3 suppresses anti-tumor immunity via the CCL2–CCR2–M2 macrophage axis and contributes**
2 **to ovarian cancer progression**

3

4 Taito Miyamoto¹, Ryusuke Murakami^{1,2*}, Junzo Hamanishi¹, Kenji Tanigaki³, Yuko Hosoe¹, Nathan
5 Mise⁴, Shiro Takamatsu¹, Yuka Mise¹, Masayo Ukita¹, Mana Taki¹, Koji Yamanoi¹, Naoki
6 Horikawa^{1,5}, Kaoru Abiko^{1,6}, Ken Yamaguchi¹, Tsukasa Baba⁷, Noriomi Matsumura⁸ and Masaki
7 Mandai¹

8

9 ¹ Department of Gynecology and Obstetrics, Kyoto University Graduate School of Medicine

10 ² Department of Gynecology, Shiga General Hospital

11 ³ Research institute, Shiga Medical Center

12 ⁴ Department of Environmental and Preventive Medicine, Jichi Medical University

13 ⁵ Department of Obstetrics and Gynecology, Shizuoka General Hospital

14 ⁶ Department of Obstetrics and Gynecology, National Hospital Organization Kyoto Medical Center

15 ⁷ Department of Obstetrics and Gynecology, Iwate Medical University School of Medicine

16 ⁸ Department of Obstetrics and Gynecology, Kindai University School of Medicine

17

18 **Running title:** B7-H3 immunosuppression via M2 macrophages in ovarian cancer

19

20 **Keywords:** Ovarian cancer, B7-H3, M2 macrophage, CCL2, tumor immunity

21

22 **Synopsis:** A role of B7-H3 in M2 macrophage-mediated immunosuppression in ovarian cancer is
23 demonstrated. The data reveal B7-H3's potential as a therapeutic target to enhance anti-tumor
24 responses in ovarian cancer, highlighting a differential role from other B7 family members.

25

26 **Financial support:** This work was supported by the Grants-in-Aid for Strategic Medical Science
27 Research (grant numbers 18K16769 and 20K18210) from the Ministry of Education, Culture, Sports,
28 Science, and Technology of Japan.

29

30 ***Corresponding author:** Ryusuke Murakami

31 Department of Gynecology, Shiga General Hospital

32 5-4-30, Moriyama, Moriyama city, Shiga 524-8524, JAPAN

33 Phone: 81-77-582-5031, Fax: 81-77-582-5931

34 E-mail: ryusukem@kuhp.kyoto-u.ac.jp

35

36 **Disclosure statement:** Taito Miyamoto was supported by Research Fellowships for Young Scientists
37 from Japan Society for the Promotion of Science. Junzo Hamanishi was supported by grants from
38 Ono Pharmaceutical, Sumitomo Dainippon Pharma, and MSD outside the submitted work. Ken

39 Yamaguchi was supported by grants from Bayer. Noriomi Matsumura was supported by personal
40 fees as an outside director from Takara Bio Inc. and grants and lecture fees from AstraZeneca
41 outside the submitted work. Masaki Mandai was supported by lecture fees from Chugai
42 Pharmaceutical, Takeda Pharmaceutical, and AstraZeneca, and grants from Chugai Pharmaceutical,
43 MSD, and Tsumura outside the submitted work. The other authors have declared no additional
44 potential conflicts of interest.

45 **Abstract**

46 New approaches beyond PD-1/PD-L1 inhibition are required to target the immunologically diverse
47 tumor microenvironment (TME) in high-grade serous ovarian cancer (HGSOC). In this study, we
48 explored the immunosuppressive effect of B7-H3 (CD276) via the CCL2–CCR2–M2 macrophage axis
49 and its potential as a therapeutic target. Transcriptome analysis revealed that B7-H3 is highly
50 expressed in PD-L1-low, non-immunoreactive HGSOC tumors, and its expression negatively
51 correlated with an IFN γ signature, which reflects the tumor immune-reactivity. In syngeneic mouse
52 models, B7-H3 (*Cd276*) knockout (KO) in tumor cells, but not in stromal cells, suppressed tumor
53 progression, with a reduced number of M2 macrophages and an increased number of IFN γ +CD8⁺ T
54 cells. CCL2 expression was downregulated in the B7-H3 KO tumor cell lines. Inhibition of the CCL2–
55 CCR2 axis partly negated the effects of B7-H3 suppression on M2 macrophage migration and
56 differentiation, and tumor progression. In HGSOC patients, B7-H3 expression positively correlated
57 with CCL2 expression and M2 macrophage abundance, and patients with B7-H3-high tumors had
58 fewer tumoral IFN γ +CD8⁺ T cells and poorer prognosis than patients with B7-H3-low tumors. Thus,
59 B7-H3 expression in tumor cells contributes to CCL2–CCR2–M2 macrophage axis-mediated
60 immunosuppression and tumor progression. These findings provide new insights into the
61 immunological TME and could aid the development of new therapeutic approaches against the
62 unfavorable HGSOC phenotype.

63 Introduction

64 Ovarian cancer is the eighth leading cause of cancer death in women worldwide, with an
65 estimated figure of more than 200,000 deaths per year (1). In addition to conventional surgery and
66 chemotherapy, the introduction of anti-VEGF and PARP inhibitors as therapeutic modalities has
67 remarkably prolonged the duration of progression-free survival, even though progression remains
68 inevitable in the majority of cases (2,3). The efficacy of PD-1/PD-L1 inhibition therapy is limited in
69 ovarian cancer, as evidenced by clinical trials, and immunotherapy has not yet become the standard
70 treatment option (4-6).

71 Of all the histological types of ovarian cancer, high-grade serous ovarian cancer (HGSOC)
72 remains the most common and the most aggressive (7,8). Although the tumor microenvironment
73 (TME) of HGSOC varies widely, it is well-characterized by four subtypes based on gene expression
74 profiles: differentiated, immunoreactive, mesenchymal, and proliferative subtypes (9,10). The
75 immunoreactive subtype is characterized as tumors with high expression of IFN γ and PD-L1, a
76 representative anti-tumor cytokine and an immunomodulatory molecule upregulated in response to
77 IFN γ , respectively, and patients have a better prognosis (10-12). The mesenchymal type is
78 characterized as epithelial-mesenchymal transition (EMT)-high, immunosuppressive tumors with
79 poor prognosis (10,13,14). The differentiated and proliferative subtypes consist of immune ‘desert’
80 tumors (14). PD-1/PD-L1 inhibition therapy is relatively effective in treating PD-L1-high
81 immunoreactive tumors. However, non-immunoreactive phenotypes, which comprise a majority of
82 HGSOC tumors, respond poorly to the treatment (4). To elucidate what contributes to the differences
83 in the TME, and new immunological approaches to treat non-immunoreactive phenotypes other than
84 PD-1/PD-L1 inhibition, are required.

85 B7-H3 is a transmembrane protein from the B7 family; it was first reported in 2001 (15).
86 Developments in therapies targeting B7-H3, including antibody–drug conjugates,
87 radioimmunotherapy, and chimeric antigen receptor T cells, which focus on its high selective
88 expression in tumor tissues, highlight the potential of B7-H3 as a therapeutic target (16-18). B7-H3
89 seems to play complex roles in modulating the TME. Not only does it exert its immunomodulatory
90 effects by directly acting on target cells as an immune checkpoint (15,19,20), it is also involved in the
91 intracellular signaling of cancer cells, such as the STAT3 pathway (21-23). Its contribution to
92 immunosuppressive TME, other than as an immune checkpoint molecule, remains to be fully
93 elucidated.

94 Here, we demonstrate that B7-H3 expression is upregulated in the non-immunoreactive
95 tumors of HGSOC and that B7-H3 contributes to ovarian cancer progression via CCL2–CCR2–M2
96 macrophage axis-mediated immunosuppression, in both mouse syngeneic ovarian cancer models and
97 HGSOC cases. Our results not only augment the current understanding of the immunological
98 heterogeneity of HGSOC but also provide a foundation for stratification of the immunosuppressive
99 HGSOC phenotype with a B7-H3-high, M2 macrophage-rich TME and facilitate the development of
100 new treatment strategies other than PD-1/PD-L1 inhibition that can specifically benefit patient

101 groups with extremely poor prognosis.

102

103 **Materials and Methods**

104 **Study approval.** This study was approved by the Kyoto University Graduate School and Faculty of
105 Medicine Ethics Committee (reference number G531) and conforms to the Declaration of Helsinki.
106 Informed consent was obtained from all participants via an opt-in approach (wherein participants
107 signed a printed informed consent document) or an opt-out approach (wherein participants were
108 informed about the study through the website). All animal studies were approved by the Kyoto
109 University Animal Research Committee.

110

111 **Human samples.** Formalin-fixed, paraffin-embedded (FFPE) primary site tumor specimens ($n=62$)
112 and fresh primary site tumor samples ($n=28$) were collected from patients with HGSOC, who
113 underwent primary surgery at the Kyoto University Hospital between 1998 and 2015. Patients
114 without primary site resection surgery or those who received chemotherapy prior to surgery were
115 excluded. Blood samples from HGSOC patients ($n=23$) and healthy female donors ($n=10$) were also
116 collected between 2012 and 2020. FFPE samples were stored at room temperature, and fresh tumor
117 samples and blood samples were stored at $-80\text{ }^{\circ}\text{C}$ until use.

118

119 **Bioinformatics analysis.** Gene expression data of 30 HGSOC specimens from the Kyoto University
120 Hospital that were partially deposited in the Gene Expression Omnibus (RRID: SCR_005012,
121 accession numbers: GSE39204 and GSE55512) were classified into the four transcriptome subtypes
122 (24), according to the Classification of Ovarian Cancer (CLOVAR) subtype signatures (10).
123 Differentially expressed genes (DEGs) between the immunoreactive ($n = 8$) and non-immunoreactive
124 ($n = 22$) subtypes were extracted using the Samroc method as described previously (25). The gene
125 expression profiles from The Cancer Genome Atlas-Ovarian Cancer (TCGA-OV) RNA-sequencing
126 dataset ($n=263$) from TCGA Data Portal (RRID: SCR_003193,
127 illuminahisecq_rnaseqv2_Level_3_RSEM_genes_normalized_data files obtained on October 19, 2015)
128 was used for comparison. Single-sample Gene Set Enrichment Analysis (ssGSEA) (26), using
129 GenePattern software (RRID:SCR_003201, version 3.5.0), was performed to evaluate the IFN γ
130 signature activity scores using the previously reported gene set (27) using R software (RRID:
131 SCR_001905, version 3.6.1).

132

133 **Cell culture and transfection.** The OV2944-HM-1 (HM-1) mouse ovarian cancer cell line was
134 purchased from RIKEN BioResource Center (RRID: SCR_003250, Cat# RCB1483; RRID:
135 CVCL_E954; Tsukuba, Japan) in January 2003. HM-1 cells were cultured and maintained in
136 minimal essential medium (MEM)-alpha (Cat# 12571063, Thermo Fisher Scientific, Waltham, MA,
137 USA) supplemented with 10% (v/v) heat-inactivated FBS (Cat# S1810, Biowest, San Marcos, TX,
138 USA) and penicillin–streptomycin (100 IU/ml penicillin and 100 $\mu\text{g}/\text{ml}$ streptomycin; Cat# 26253-84,
139 Nacalai Tesque, Kyoto, Japan) in an atmosphere of 5% CO $_2$ at 37 $^{\circ}\text{C}$. The ID8 mouse ovarian cancer
140 cell line was kindly provided by Dr. Katherine Roby of The University of Kansas Medical Center

141 (RRID: CVCL_IU14) in September 2009. Human ovarian cancer cell lines OVCAR3 (RRID:
142 CVCL_0465) and OVCA420 (RRID: CVCL_3935) were kindly provided by Dr. Susan K. Murphy of
143 Duke University in June 2007. Both ID8 and human ovarian cancer cells were cultured and
144 maintained in RPMI1640 medium (Invitrogen, Carlsbad, CA, USA) supplemented with 10% FBS
145 and penicillin–streptomycin in an atmosphere of 5% CO₂ at 37 °C. All cell line-based experiments
146 were performed before passage 20. All cell lines were regularly tested for mycoplasma contamination
147 (date of last check: April 12, 2021) using a Mycoplasma PCR Detection Kit (Cat# G238; Applied
148 Biological Materials, Richmond, BC, Canada). Human cell lines (OVCAR3 and OVCA420) were
149 re-authenticated on April 14, 2021, by short tandem repeat analysis.

150 For CRISPR/Cas9-mediated *Cd276* knockout (B7-H3 KO), target sequences were
151 determined as previously described (16). Three single-guide RNAs (sgRNAs) and a control sgRNA
152 were synthesized by FASMAC (Kanagawa, Japan). A mixture of the RNAs and Guide-it recombinant
153 Cas9 (Cat# 632641, Takara Bio Inc., Shiga, Japan) was transfected into the HM-1 and ID8 cells
154 using the TransIT-X2 Dynamic Delivery System (Cat# MIR6003, Mirus Bio, Madison, WI, USA). The
155 cells were incubated with rabbit anti-CD276 (1:1000 dilution, clone: EPNCIR122, Cat# ab134161;
156 RRID: AB_2687929, Abcam, Cambridge, UK) for 20 min at 4 °C and with Goat Anti-Rabbit IgG H&L
157 (Alexa Fluor 647) (1:2000 dilution, Cat# ab150079; RRID:AB_2722623, Abcam) for 10 min at 4 °C.
158 Alexa Fluor 647-negative cell populations were sorted by flow cytometry using BD FACSAria II Cell
159 Sorter (RRID: SCR_018934, BD Biosciences, Franklin Lakes, NJ, USA). The purity of Alexa Fluor
160 647-negative cells was >99 %. Single cells were isolated by limiting dilution and cultured again on
161 96-well plates (Cat# 655180, Greiner Bio-One, Kremsmunster, Austria) for 8 days under the same
162 conditions described in the section above, followed by expansion. Finally, B7-H3 expression
163 deficiency was confirmed using FACS analysis and quantitative PCR (qPCR).

164 B7-H3-knockdown HGSOC cells, OVCAR3-sh-B7-H3 and OVCA420-sh-B7-H3, and their
165 control cells were generated by lentiviral-mediated transfection with short hairpin RNAs (shRNAs)
166 targeting B7-H3 or a non-silencing control (sh1, Cat# TRCN0000128599; sh2, Cat#
167 TRCN0000436667; sh control, Cat# SHC002; Sigma-Aldrich, St. Louis, MO, USA). The sgRNA and
168 shRNA sequences are listed in Supplementary Table S1.

169
170 **Mice.** Five- to six-week-old female C57BL6 (strain code: 027) and B6C3F1 (C57BL6×C3/He F1, strain
171 code: 031) mice were purchased from CLEA Japan (Tokyo, Japan) and used in immunocompetent
172 mouse experiments. Five- to six-week-old female BALB/c-nu (*Foxn1^{nu}*, strain code: 194) mice were
173 purchased from CLEA Japan and used in immunodeficient mouse experiments. The C57BL6
174 background *Cd276^{-/-}* (B7-H3 KO) mice were kindly provided by Dr. Brad St. Croix of the National
175 Cancer Institute. Animals were maintained under specific pathogen-free conditions.

176
177 **Tumor models.** A total of 1×10^6 HM-1-B7H3 KO cells or control cells were inoculated intradermally
178 into the shaved abdominal lesion of B6C3F1 and nude mice. A total of 5×10^5 HM-1-B7H3 KO or

179 control cells were injected into the abdominal cavity of B6C3F1 or nude mice (intraperitoneal model).
180 Similarly, 5.0×10^6 ID8 B7-H3 KO or control cells were injected into the abdominal cavity of C57BL6
181 or nude mice (intraperitoneal model). Intradermal tumor size was measured using calipers and
182 calculated as follows: volume = length \times width \times height \times $\pi/6$. In the intraperitoneal models, tumor
183 growth was evaluated based on changes in body weight, which reflect the amount of ascites and
184 omental tumor weight. Survival analysis was also performed in these models. Intradermal tumor
185 size and body weight were measured once or twice a week. Intradermal tumors of HM-1-B7H3 KO or
186 control cells at days 10, 12, and 25 were used for RNA-sequencing, flow cytometry,
187 immunohistochemistry, and ELISA, respectively. Intraperitoneal tumors of ID8-B7H3 KO or control
188 cells at days 63 and 67 were used for ELISA and flow cytometry, respectively. For B7-H3 KO mouse
189 studies, only *Cd276*^{+/+} and *Cd276*^{-/-} littermates derived from *Cd276* heterozygous intercrosses were
190 used for comparison. The CCR2 antagonist (RS504393: 2 mg/kg body weight; Cat# 17330, Cayman
191 Chemical, Ann Arbor, MI, USA) treatment was initiated a day after tumor cell inoculation and was
192 administered intraperitoneally daily. Mice were euthanized before becoming moribund.

193

194 **Cell treatments.** OVCAR3 and OVCA420 human ovarian cancer cells (1×10^5) were cultured in
195 6-well plates (Cat# 657160, Greiner Bio-One) as described in the “Cell culture and transfection”
196 section above and treated with 20 ng/mL recombinant IFN γ (Cat# 570202, BioLegend, San Diego, CA,
197 USA) (28) or 0.1 % bovine serum albumin (BSA; Cat# 7284, Sigma-Aldrich, St. Louis, MO, USA) as a
198 control the following day. Cells were analyzed for the expression of B7-H3 (*CD276*), PD-L1 (*CD274*),
199 and PD-L2 (*PDCD1LG2*) using qPCR and flow cytometry (as described below) after treatment for 24
200 and 48 hours, respectively.

201 For STAT3 inhibition, 1×10^5 cells were treated with the STAT3 inhibitor C188-9 (Cat# S8605,
202 Selleck Chemicals, Houston, TX, USA) for the mouse cell lines HM-1 and ID8 (29) or with Stattic
203 (Cat# ab120952, Abcam, Cambridge, UK) for the human cell lines OVCAR3 and OVCA420 (30) at
204 1.25 μ M and 5 μ M for 24 h, respectively. *Ccl2* and *CCL2* expression levels were analyzed using qPCR
205 as described below.

206

207 **Tumor cell proliferation assay.** HM-1-B7H3 KO cells, ID8-B7-H3 KO cells, or their respective control
208 cells were seeded in 96-well plates at 1×10^3 cells/well (Greiner Bio-One) and incubated for 3 days in
209 an atmosphere of 5% CO $_2$ at 37 °C. The number of viable cells in each well was examined every 24 h
210 by absorbance at 450 nm using Cell Count Reagent SF (Cat# 07553-44, Nacalai Tesque) and iMark
211 microplate reader (Cat# 168-1130J, Bio-Rad, Hercules, CA, USA). Absorbance values at 72h were
212 compared using Microsoft Excel (RRID: SCR_016137, Redmond, WA, USA).

213

214 **Macrophage and monocyte selection.** For tumor-derived macrophage selection, single cells from the
215 tumors were prepared as described in the “Flow cytometry” section below. F4/80-positive
216 macrophages were positively selected using anti-Mouse F4/80 PE antibody (clone: BM8, Cat#

217 123109; RRID: AB_893498, Biolegend), EasySep Mouse PE positive selection kit II (Cat# 17666,
218 Stemcell Technologies, Vancouver, BC, Canada), and EasySep Magnet (Cat# 18000, Stemcell
219 Technologies). The purity of F4/80-positive cells was >90% as confirmed by flow cytometry. For mouse
220 monocyte selection, single cells from the bone marrow of the femur and tibia of B6C3F1 or C57BL6
221 non-tumor-bearing mice were collected by mechanical dissociation. For human monocyte selection,
222 peripheral blood mononuclear cells of healthy donors were separated using Leucosep (Cat# 227290,
223 Greiner) and Lymphosep (Cat# 1692254, MP Biomedicals, Santa Ana, CA, USA). Ly6C-positive
224 mouse monocytes and CD14-positive human monocytes were positively selected by EasySep Magnet
225 as described above using anti-Mouse Ly6C PE antibody (clone: HK1.4, Cat# 128007; RRID:
226 AB_1186133, Biolegend) and anti-Human CD14 PE antibody (clone: M5E2, Cat# 301806; RRID:
227 AB_314188, Biolegend). The purity of Ly6C-positive and CD14-positive cells was >90%, respectively,
228 as confirmed by flow cytometry.

229

230 **RNA extraction and reverse transcription (RT) qPCR.** Human (OVCAR3 and OVCA420) and mouse
231 (HM-1 and ID8) cells or macrophages isolated from the tumors of HM-1-B7H3 KO or control cells (as
232 described in the preceding section) were lysed in RLT buffer (Cat# 1015750, Qiagen, Hilden,
233 Germany) containing 1% 2-mercaptoethanol (Cat# 1610710, Bio-Rad). Intradermal tumors of
234 HM-1-B7H3 KO cells or control cells were treated in a bead homogenizer with RLT buffer and
235 centrifuged at 16,000 $\times g$ for 1 min at 4 °C. Total RNA was extracted from the lysates using RNeasy
236 Mini Kit (Cat# 74104, Qiagen).

237 A ReverTra Ace qPCR RT Kit (Cat# FSQ-101, TOYOBO, Osaka, Japan) was used for cDNA
238 synthesis. Gene amplification was performed using PowerUp SYBR Green Master Mix (Cat# A25742,
239 Thermo Fisher Scientific, Waltham, MA, USA) on a StepOne Plus real-time PCR system (Applied
240 Biosystems, Foster City, CA, USA). Fifty nanograms of RNA was used as the template for PCR to
241 detect the relative expression levels of *CD276*, *CD274* (PD-L1), *PTCD1LG2* (PD-L2), and *CCL2* for
242 human cells, and *Cd276*, *Ccl2*, *Arg1*, *Il10*, and *Ifng* for mouse cells; the primer sequences are listed in
243 Supplementary Table S1. Relative expression levels were calculated using the $2^{-\Delta\Delta Ct}$ method.
244 *GAPDH/Gapdh* was used for normalization.

245

246 **Immunostaining and evaluation.** FFPE sections of the 62 HGSOE samples and 3–6 mouse tumors of
247 HM-1-B7H3 KO cells or control cells were immunostained as described previously (31). Epitope
248 retrieval was performed at 120 °C for 10 minutes using citrate buffer at pH 6.0 (B7-H3) or Tris-EDTA
249 buffer at pH 9.0 (α SMA, CD206, CD8, and IFN γ). The kits, antibodies and dilutions used are listed in
250 Supplementary Table S2. Tumor cell B7-H3 expression was evaluated as previously described (32)
251 and scored as follows: 0, negative or very weak; 1, weak; 2, moderate, and 3, strong (16). Scores of 0/1
252 and 2/3 were defined as B7-H3-low and B7-H3-high, respectively. Tumor-infiltrating CD206⁺ cells
253 (200 \times) were counted from five fields, and the average number of cells was calculated. For the
254 evaluation of CD8⁺ and IFN γ ⁺CD8⁺ T cells, the number of cells in the representative CD8⁺ cell-rich

255 field was counted at 200× magnification. The sensitivity and specificity of the IFN γ antibody was
256 confirmed using appendix (Cat# CS802695, OriGene, Rockville, MD, USA) and tonsil (kindly
257 provided by Kyoto University Department of Otolaryngology, Head and Neck Surgery) tissue as
258 positive controls (Supplementary Figure S1a-b). Slides were analyzed using a BZ 9000 fluorescence
259 microscope (RRID: SCR_015486, Keyence, Osaka, Japan).

260

261 **Flow cytometry.** IFN γ - or BSA-treated OVCAR3 and OVCA420 cells, HM-1-B7H3 KO cells and
262 ID8-B7-H3 KO cells or their respective control cells, and OVCAR3-sh-B7-H3 and
263 OVCA420-sh-B7-H3 or their respective control cells were collected from the culture plates using
264 trypsin (Cat# T4549, Sigma-Aldrich) and incubated for 20 min at 4 °C with the corresponding
265 antibodies listed in Supplementary Table S2. Tumors of HM-1-B7H3 KO cells, ID8-B7-H3 KO cells,
266 or their control cells were minced into thin pieces and dissociated in 100 μ g/mL of DNase I (Cat#
267 11284932001, Roche, Basel, Switzerland) and 1 mg/mL of collagenase IV (Cat# CLS4, Worthington,
268 Columbus, OH, USA) in RPMI 1640 medium. The tissues were incubated for 1 h at 37 °C with
269 agitation. Single cells were prepared through a 70 μ m nylon mesh strainer (Cat# 542070, Greiner
270 Bio-One). FcR blocking for leukocytes was performed with FcR Blocking Reagent (for mouse samples:
271 Cat# 130-092-575, RRID: AB_2892833; for human samples: Cat# 130-059-901, RRID: AB_2892112,
272 Miltenyi Biotec, Bergisch Galdbach, Germany) for 10 min at 4 °C. Tumor-infiltrating immune cells
273 were stained to detect CD4 $^+$ T cells (CD3 $^+$ CD4 $^+$ CD8 $^-$), CD8 $^+$ T cells (CD3 $^+$ CD4 $^-$ CD8 $^+$), M2
274 macrophages (CD45 $^+$ F4/80 $^+$ CD206 $^+$), M1 macrophages (CD45 $^+$ F4/80 $^+$ CD80 $^+$ or CD45 $^+$ F4/80 $^+$ CD86 $^+$),
275 and dendritic cells (DCs, CD45 $^+$ CD11c $^+$ MHC class 2 $^+$) (33) with the antibodies listed in
276 Supplementary Table S2 for 30 min at 4 °C. Gating strategies for each cell subset are shown in
277 Supplementary Figure S2. For IFN γ staining, single cells from the tumor were incubated for 4 h with
278 eBioscience Cell Stimulation Cocktail (Cat# 00-4970-93, Invitrogen, Carlsbad, CA, USA) and for 2 h
279 with Brefeldin A (Cat# B7651, Sigma-Aldrich). BD Cytofix/Cytoperm Fixation/Permeabilization Kit
280 (Cat# 554714, BD Biosciences) was used for intracellular staining. Non-viable cells were stained
281 with 7-amino-actinomycin D (AAD) solution (Cat# 51-68981E, BD Biosciences) or DAPI solution
282 (Cat# D1306, Life Technologies, Carlsbad, CA, USA) and gated out. MACS Quant Analyzer 10
283 (Miltenyi Biotec) and FlowJo (RRID: SCR_008520, FlowJo LLC, Ashland, OR, USA) were used for
284 analysis.

285

286 **T-cell proliferation assay.** For T-cell selection, single cells from the spleens of B6C3F1 mice bearing
287 tumors of HM-1-B7H3 KO cells or control cells harvested at day 12 were collected by mechanical
288 dissociation. Red blood cells were lysed with Pharm Lyse buffer (Cat# 555899, BD Bioscience). The
289 purity of CD3 $^+$ cells was >90% as confirmed by flow cytometry. T cells were negatively selected using
290 mouse Pan-T-cell isolation kit II (Cat# 130-095-130, Miltenyi Biotec), an LS column (Cat#
291 130-042-401, Miltenyi Biotec), and QuadroMACS Separator (Cat# 130-090-976, Miltenyi Biotec).

292 T cells were labeled using 10 mmol/L carboxyfluorescein succinimidyl ester (CFSE; Cat#

293 600121, Cayman Chemical). T cells (1×10^5) were co-cultured with F4/80⁺ macrophages (obtained as
294 described in the “Macrophage and monocyte selection” section above) at 2:1, 4:1, and 8:1 ratios with
295 RPMI 1640 medium supplemented with 10% FBS, 2 mM of L-glutamine (Cat# 25030-081, Gibco),
296 and 50 μ M of 2-mercaptoethanol for 72 h in an atmosphere of 5% CO₂ at 37 °C. During incubation, T
297 cells were activated with Dynabeads Mouse T-activator CD3/28 (1:100 dilution, Cat# 11453D,
298 Thermo Fisher Scientific). Activated T cells without macrophages were used as a positive control.
299 After 72 hours, T-cell proliferation was examined using flow cytometry according to the decrease of
300 the CFSE fluorescence intensity. MACS Quant Analyzer 10 (Miltenyi Biotec) and FlowJo (FlowJo)
301 were used for analysis. The culture supernatants were collected and used for ELISA.

302

303 **ELISAs.** Mouse IFN γ levels in the cell culture supernatant of T cells co-cultured with macrophages
304 were measured using Mouse IFN- γ Quantikine ELISA Kit (Cat# MIF00, R&D Systems). HM-1-B7H3
305 KO cells, ID8-B7-H3 KO cells or their control cells, and OVCAR3-sh-B7-H3 and OVCA420-sh-B7-H3
306 or their control cells were seeded at a density of 1×10^5 with 500 μ L of the corresponding medium
307 (see “Cell culture and transfection” section) in 24-well plates (Cat# 662160, Greiner Bio-One). Cell
308 culture supernatants were collected after 24 h with a 0.45 μ m Millex filter (Cat# SLHVR33RS,
309 Merck Millipore, Burlington, MA, USA) and used for ELISA. These supernatants were also used for
310 migration and monocyte differentiation assays (described in detail below) as the tumor
311 cell-conditioned medium (TCM). Human and mouse tumor tissues were treated in a bead
312 homogenizer, and sonicated in 1 \times RIPA buffer (Cat# 89900, Thermo Fisher Scientific) containing a
313 protease inhibitor cocktail (Cat# 03969-21, Nacalai Tesque) and a phosphatase inhibitor cocktail
314 (Cat# 07575-51, Nacalai Tesque), followed by centrifugation at 16,000 $\times g$ for 5 min at 4 °C. Human
315 tumor lysates were used for B7-H3 and CCL2 detection at 75 μ g and 200 μ g as protein amount,
316 respectively, and 20 μ g as protein amount of mouse tumor lysates were used for CCL2 detection.
317 Mouse CCL2 protein levels in culture supernatants and tumor lysates were measured using the
318 Mouse CCL2/JE/MCP1 DuoSet kit (Cat# DY479-05, R&D Systems). Human CCL2 protein levels in
319 culture supernatants, tumor lysates, and serum samples were measured using Human CCL2/MCP-1
320 Quantikine ELISA Kit (Cat# DCP00, R&D Systems). Human B7-H3 protein levels in tumor lysates
321 were measured using Human B7-H3 Quantikine ELISA Kit (Cat# DB7H30, R&D Systems). The
322 absorbance readings at 570 nm were subtracted from the readings taken at 450 nm using an iMark
323 microplate reader (Bio-Rad) to establish standard curves for calculation of the concentration.
324 Microsoft Excel was used for analysis.

325

326 **Immunoblotting.** Nuclear proteins were collected from HM-1-B7H3 KO cells, ID8-B7-H3 KO cells or
327 their control cells, and OVCAR3-sh-B7-H3 and OVCA420-sh-B7-H3 or their control cells using
328 NE-PER nuclear and cytoplasmic extraction reagents (Cat# 78833, Thermo Fisher Scientific).
329 Protein (20 μ g) of HM-1-B7H3 KO cells or their control cells, and 10 μ g protein of the other cells were
330 loaded onto 8% acrylamide gels. Proteins were subsequently separated using SDS-PAGE and

331 transferred onto PVDF membranes (Cat# 1620177, Bio-Rad). After blocking for 1 h with Blocking
332 One-P (Cat# 05999-84, Nacalai Tesque), the membranes were then immunoblotted with the
333 antibodies listed in Supplementary Table S2 at the indicated dilutions. The membranes were
334 incubated with the primary antibody overnight at 4 °C and with the secondary antibody for 1 h at
335 room temperature. Bands were visualized using ChemiDoc XRS+ Systems (Bio-Rad). Signals were
336 quantified using Image Lab 2.0 (RRID: SCR_014210, Bio-Rad).

337

338 **RNA-sequencing.** Total RNA from HM-1-B7H3 KO cells, ID8-B7-H3 KO cells or their control cells, or
339 intradermal tumors of HM-1-B7H3 KO cells or their control cells at day 10 of tumor growth were
340 extracted as described in the ‘RNA extraction and reverse transcription (RT) qPCR’ section and used
341 for RNA-sequencing. Sequencing was performed on an Illumina NovaSeq 6000 platform (RRID:
342 SCR_016387, Illumina) to generate 100 bp paired-end reads. Raw reads were trimmed using Trim
343 Galore (RRID: SCR_011847), and the resulting reads were aligned to the mouse reference genome
344 GRCm38/mm10 using STAR (RRID: SCR_004463). Differential expression analysis was performed
345 using DESeq2 (RRID: SCR_015687) between control ($n=3$) and B7-H3 KO ($n=3$) groups of the ID8
346 and HM-1 cell lines, and HM-1 intradermal tumors (processed as indicated in above sections). After
347 excluding the genes showing low expression and low fold change between groups (“baseMean” >
348 1000; $|\log_2\text{FoldChange}| > 2$; $p_{adj} < 0.01$), the remaining genes were considered as DEGs and listed
349 in Supplementary Tables S3–S5. RNA-sequence data have been deposited in the Gene Expression
350 Omnibus database, under accession number GSE174137.

351

352 ***In vitro* M2 macrophage generation.** Mouse and human monocytes (obtained as described in the
353 “Macrophage and monocyte selection” section) were cultured in 6-well plates (Cat# 657160, Greiner
354 Bio-One) at 3×10^6 cells/well and 6×10^5 cells/well, respectively, with RPMI 1640 medium
355 supplemented with 40 ng/mL of M-CSF (mouse: Cat# 576402, human: Cat# 574802, BioLegend, San
356 Diego, CA, USA) and 40 ng/mL of IL6 (mouse: Cat# 216-16, PeproTech, Cranbury, NJ, USA, human:
357 Cat# 570802, BioLegend) for 6–7 days in an atmosphere of 5% CO₂ at 37 °C and used for migration
358 assays. After incubation, >70% of the cultured mouse cells were F4/80-positive and CD206-positive,
359 and >85 % of the cultured human cells were CD206-positive as confirmed by flow cytometry.

360

361 **Migration assays.** Monocytes or the generated M2 macrophages (mouse: 1×10^5 cells, human: 5×10^4
362 cells, isolated as described in the “Macrophage and monocyte selection” and “*In vitro* M2 macrophage
363 generation” sections, pretreated with 2 μM RS504393 (described in “Tumor models”) or DMSO were
364 plated in the upper compartment of 8 μm cell culture insert (Cat# 353097, Corning, Corning, NY,
365 USA), and 500 μL of TCM of HM-1-B7H3 KO cells, ID8-B7-H3 KO cells or their control cells, and
366 OVCA420-sh-B7-H3 or their control cells (generated as described in the “ELISAs” section) was added
367 to the lower compartment. Plates were incubated for 1 hour in an atmosphere of 5% CO₂ at 37 °C,
368 and migrated cells were counted using CountBright Absolute Counting beads (Cat# 36950, Thermo

369 Fisher Scientific).

370

371 **Monocyte differentiation assay.** Mouse bone marrow monocytes (isolated and cultured as described in
372 the “Macrophage and monocyte selection” section) were plated in the upper compartment of 0.4 μ m
373 cell culture inserts (Cat# 353095, Corning) at a density of at 1×10^5 , and 500 μ L of TCM of
374 HM-1-B7H3 KO cells, ID8-B7-H3 KO cells or their control cells (generated as described in the
375 “ELISAs” section) supplemented with 20 μ g/mL anti-mouse CCL2 (Cat# AB-479-NA,
376 RRID:AB_354366; R&D Systems, Minneapolis, MN, USA) or goat IgG control (Cat# AB-108-C,
377 RRID:AB_354267; R&D Systems) was added to the lower compartment. Plates were incubated for 72
378 hours in an atmosphere of 5% CO₂ at 37 °C, and F4/80+CD206+ cells were then evaluated using flow
379 cytometry, as described above.

380

381 **Statistics.** At least three *in vitro* experiments and at least two *in vivo* experiments were
382 independently performed. Data from one representative experiment are presented. For mouse
383 experiments, cages of mice were randomly allocated to the experimental groups. Sample sizes were
384 chosen to assure reproducibility of the experiments in accordance with the replacement, reduction,
385 and refinement principles of the animal ethics regulation. Grouped data are shown as the average \pm
386 standard error of the mean (SEM) in all figures except non-normally distributed data for clinical
387 samples, which shows the median with 95 % confidence intervals. The investigator was not blinded
388 to the group allocation. *A priori* power analysis was not performed for human samples. Survival
389 curves were constructed using the Kaplan-Meier method. Prognostic factors for progression-free
390 survival (PFS) and overall survival (OS) of HGSOC patients were assessed by univariate and
391 multivariate analysis using the Cox proportional hazards regression model. Statistical analysis was
392 performed using R software and GraphPad Prism 7 (RRID: SCR_002798, GraphPad Software, San
393 Diego, CA, USA), and the appropriate tests are indicated in the figure legends. Significance was set
394 as * $P < 0.05$, ** $P < 0.01$, and *** $P < 0.001$.

395 Results

396 B7-H3 expression is upregulated in the non-immunoreactive TME of HGSOC

397 We first identified the genes acting antagonistic to the immunoreactive TME in HGSOC
398 based on our RNA expression array data. *CD276* (B7-H3) was the most upregulated gene in the
399 non-immunoreactive subtype (Figure 1a). Analysis of TCGA-OV revealed that B7-H3 expression was
400 higher in the proliferative and mesenchymal subtypes than in the immunoreactive subtypes
401 ($P=0.004$ and $P<0.001$, Figure 1b). Among the T-cell suppressive immune checkpoint molecules of the
402 B7 family, only B7-H3 expression was lower in the immunoreactive subtype and higher in the
403 non-immunoreactive subtype (both $P<0.001$, Figure 1c).

404 A clear positive correlation was observed between the IFN γ signature, which is a major
405 characteristic of the immunoreactive tumors and can be used as an index for predicting the
406 therapeutic efficacy of immune checkpoint inhibitor (ICI) treatment (27), and the other B7 family
407 molecules. By contrast, the IFN γ signature negatively correlated with B7-H3 expression ($P=0.020$,
408 Figure 1d). Based on the response to IFN γ , we performed qPCR or flow cytometry and observed
409 significantly increased expression of PD-L1 and PD-L2 and unchanged or slightly decreased
410 expression of B7-H3 in HGSOC cell lines (Supplementary Figure S3a-b). Moreover, PD-L1
411 expression negatively correlated with B7-H3 expression (Supplementary Figure S3c). These results
412 indicate that B7-H3 expression is associated with the non-immunoreactive TME and that B7-H3 is
413 involved in immunosuppression, albeit via a different mechanism than that of PD-L1.

414

415 B7-H3 mediates murine ovarian cancer growth via immune system regulation

416 To investigate the function of B7-H3 in tumor cells, we generated three B7-H3 knockout
417 (KO) HM-1 and ID8 mouse ovarian cancer cell lines using CRISPR-Cas9. Both cell lines express
418 B7-H3 and are resistant to PD-1/PD-L1 inhibition therapy (34,35). We confirmed B7-H3 knockout by
419 flow cytometry and immunostaining (Figure 2a-b, Supplementary Figure S4a). B7-H3 KO did not
420 affect cell proliferation *in vitro* (Supplementary Figure S4b). In immunocompetent mice, B7-H3 KO
421 delayed the growth of HM-1 intradermal and intraperitoneal tumors, as well as ID8 intraperitoneal
422 tumors (Figure 2c-d, Supplementary Figure S4c). B7-H3 suppression significantly prolonged the
423 survival of mice with ID8 tumors, a trend that was also observed with HM-1 tumors (Supplementary
424 Figure S5a). By contrast, in immunodeficient mice, tumor growth and survival were not affected by
425 B7-H3 expression in either HM-1 or ID8 cells (Figure 2e-f, Supplementary Figure S5b). These data
426 suggest that B7-H3 is involved in tumor development via immune-related mechanisms. Next, to
427 verify the role of B7-H3 in stromal cells, we injected ID8 cells into *CD276* knockout (B7-H3 KO) mice
428 and observed that B7-H3 expression did not significantly affect tumor development (Supplementary
429 Figure S6). Overall, these results indicate that B7-H3 expression in tumor cells is important for
430 tumor progression.

431

432 B7-H3 suppression reduces M2 macrophages and increases T cell-produced IFN γ in the TME

433 First, we confirmed a direct T-cell suppressive effect of tumor cell B7-H3 *in vitro*
434 (Supplementary Figure S7a-c), which has been reported in several studies (19, 20). Next, we
435 evaluated tumor-infiltrating immune cells. Although there was no difference in the number of CD8⁺
436 T cells, CD206⁺ M2 macrophages decreased in HM-1 B7-H3 KO tumors (Figure 3a, Supplementary
437 Figure S8a). Flow cytometry showed that F4/80⁺CD206⁺ M2 macrophages decreased in HM-1 B7-H3
438 KO tumors, whereas M1 macrophages, CD8⁺ T cells, CD4⁺ T cells, and DCs were unchanged (Figure
439 3b). ID8 tumors similarly showed a decrease in M2 macrophages but no change in M1 macrophages
440 (Supplementary Figure S8b). These results suggest that B7-H3 KO tumors are not only associated
441 with a decreased number of M2 macrophages within tumor tissues, but also alters macrophage
442 polarization (i.e., a decrease in the immunosuppressive fraction).

443 In macrophages from the B7-H3 KO tumors, we observed decreased expression of the M2
444 markers *Arg1* and *Ii10* but unchanged expression of the M1 marker *Ifng* (Figure 3c). T-cell
445 proliferation assays with CD3/CD28-activated T cells co-cultured with tumor-derived macrophages
446 showed that macrophages from the B7-H3 KO tumors had reduced ability to inhibit T-cell
447 proliferation compared with those from control tumors (Figure 3d), and IFN γ production in
448 co-culture supernatants was increased (Figure 3e). We also observed an increased number of
449 IFN γ ⁺CD8⁺ T cells in B7-H3 KO tumors (Figure 3f). These results suggest that B7-H3 suppression in
450 tumor cells reduces immunosuppression in the TME by not only attenuating direct T cell inhibition,
451 but also reducing the number of M2 macrophages, which may contribute to the increased IFN γ
452 production by CD8⁺ T cells and enhanced anti-tumor immunity.

453

454 **B7-H3 suppression downregulates CCL2 production in tumor cells, partly via the STAT3 pathway**

455 Next, we elucidated the mechanism by which B7-H3 suppression in tumor cells reduced M2
456 macrophage infiltration. Using RNA-sequencing, we found 90, 131, and 67 DEGs in the HM-1 and
457 ID8 cell lines and HM-1 intradermal tumors relative to controls, respectively (Supplementary Tables
458 S3–S5). We identified *Ccl2* as a common downregulated gene in the KO groups (Figure 4a). We also
459 confirmed that changes in expression of several chemokines related to T-cell trafficking were not
460 consistent between the cell lines and the B7-H3 KO tumors (Supplementary Figure S9). A reduction
461 in CCL2 protein in the B7-H3 KO groups was confirmed in both culture supernatants and tumor
462 lysates from HM-1 and ID8 cells (Figure 4b-c). Then, we investigated whether B7-H3 suppression
463 also altered CCL2 in human HGSOC cell lines (Supplementary Figure S10) and confirmed a
464 decrease in CCL2 in the culture supernatants of the shB7-H3 cells (Figure 4d).

465 To investigate the mechanism by which B7-H3 suppression induced CCL2 downregulation,
466 we examined STAT3 (21-23) and NF- κ B (36) pathways, which have been reported as downstream
467 pathways of B7-H3. Western blots showed that phosphorylated STAT3 was decreased in the
468 B7-H3-suppressed cells (Figure 4e-f). In contrast, phosphorylated p65, a major factor in the classical
469 NF- κ B pathway, was decreased in ID8 and OVCAR3 cell lines; thus, consistent results were not
470 observed among cell lines (Supplementary Figure S11a-b). Next, we examined whether the decrease

471 in phosphorylated STAT3 contributed to CCL2 downregulation. Treatment with STAT3 inhibitors
472 C188-9 for mouse cells (29) and Stattic for human cells (30) led to a decrease in CCL2 expression
473 (Figure 4g-h). These results indicate that B7-H3 suppression downregulates the production of CCL2
474 partly via the STAT3 pathway.

475

476 **The CCL2–CCR2–M2 macrophage axis is involved in B7-H3-mediated tumor growth**

477 We confirmed whether the CCL2–CCR2 axis contributed to the effects of B7-H3 suppression
478 on M2 macrophage migration and differentiation both *in vitro* and *in vivo*. Compared with controls,
479 the migration of monocytes and M2 macrophages was reduced in the B7-H3 KO TCM, and
480 pretreatment of target cells with a CCR2 inhibitor (RS504393) partially eliminated this effect
481 (Figure 5a, Supplementary Figure S12a-b). M2 macrophage polarization was significantly reduced in
482 B7-H3 KO TCM, and this effect was partially abrogated by CCL2 antibodies (Figure 5b,
483 Supplementary Figure S12c). These results indicate that B7-H3 suppression in tumor cells reduces
484 monocyte migration and macrophage differentiation into the M2 phenotype *in vitro*, and that the
485 CCL2–CCR2 axis is responsible for these effects.

486 In the HM-1 model, CCR2 inhibition suppressed tumor growth in controls but did not affect
487 B7-H3 KO tumors (Figure 5c). Flow cytometry showed that CCR2 inhibition reduced the number of
488 M2 macrophages and increased the number of IFN γ ⁺CD8⁺ T cells in control tumors but had no effect
489 on B7-H3 KO tumors (Figure 5d). The number of total CD8⁺ T cells was not changed by the
490 treatment in either control or B7-H3 KO tumors. These results indicate that CCL2 downregulation
491 induced by B7-H3 suppression contributes to the reduction of M2 macrophages and the increase in
492 IFN γ ⁺CD8⁺ T cells *in vivo*, and that the CCL2–CCR2 axis and M2 macrophages partly contribute to
493 B7-H3-mediated tumor progression.

494

495 **Poor prognosis of B7-H3-high HGSOc with an M2 macrophage-rich, IFN γ ⁺CD8⁺ T cells-sparse TME**

496 Lastly, we investigated the relationships among B7-H3 and CCL2, M2 macrophages, CD8⁺ T
497 cells, and IFN γ ⁺CD8⁺ T cells in HGSOc clinical samples. B7-H3 and CCL2 protein in HGSOc
498 primary tumors positively correlated ($P=0.040$, Figure 6a). Serum CCL2 was elevated in HGSOc
499 patients compared with those in healthy donors ($P<0.001$, Supplementary Figure S13a); however,
500 there was no significant correlation between serum CCL2 and tumor B7-H3 ($P=0.089$,
501 Supplementary Figure S13b).

502 FFPE specimens from the primary tumor site of HGSOc cases were evaluated for tumor cell
503 B7-H3 and CD206⁺ cells by immunohistochemistry and CD8⁺ and IFN γ ⁺CD8⁺ cells by
504 immunofluorescence (Figure 6b). A positive correlation between B7-H3 expression and the number of
505 CD206⁺ M2 macrophages was observed ($P=0.018$, Figure 6c). The number of CD8⁺ T cells and
506 IFN γ ⁺CD8⁺ cells positively correlated ($P<0.001$, Figure 6d). There was no difference in the number
507 of CD8⁺ T cells in the B7-H3-high and B7-H3-low groups; however, the number of IFN γ ⁺CD8⁺ cells
508 was significantly lower in B7-H3-high versus B7-H3-low tumors ($P=0.047$, Figure 6e). Patient

509 characteristics are shown in Supplementary Table S6. Higher B7-H3 expression was a potential poor
510 prognostic factor for both PFS and OS in the univariate analysis, although it was not identified as an
511 independent prognostic factor in the multivariate analysis (Figure 6f, Supplementary Table S7).
512 These results show the immunosuppressive properties of B7-H3 in relation to M2 macrophages and
513 IFN γ ⁺CD8⁺ T cells in HGSOc patients.

514 **Discussion**

515 In this study, we investigated B7-H3 upregulation in the non-immunoreactive subtype of
516 HGSOE and hypothesized that B7-H3 exerted immunosuppressive effects via a mechanism distinct
517 from that of other B7 family members, such as PD-L1, overexpressed in immunoreactive tumors. We
518 showed that B7-H3, which has been mainly reported to directly modulate T-cell function (15,19,20),
519 similar to other immune checkpoint molecules, is involved in indirect T-cell suppression via the
520 CCL2–CCR2–M2 macrophage axis.

521 Several studies have investigated the relationship between B7-H3 and M2 macrophages.
522 B7-H3 promotes the *in vitro* differentiation of macrophages into the M2 phenotype in co-cultures of
523 HepG2 hepatoma cells and THP-1 macrophages (37) and cultures of PBMC-derived monocytes in
524 colon cancer cell culture supernatants (38); however, the underlying mechanism has not yet been
525 clarified. In an immunocompetent transgenic mouse model of head and neck cancer, anti-B7-H3
526 treatment reduces the number of immature myeloid cells, including macrophages, in the tumor and
527 activates anti-tumor immunity (32). However, whether the decreased number of macrophages was
528 an effect of anti-B7-H3 on tumor cells or on macrophages expressing B7-H3 was not clarified. To the
529 best of our knowledge, this is the first study to demonstrate that CCL2 downregulation following
530 B7-H3 suppression in tumor cells contributes to the reduction in M2 macrophages and the
531 subsequent improvement in anti-tumor responses both *in vitro* and *in vivo*. Using clinical tumor
532 samples, we also clarified the relationship of B7-H3 with CCL2 and M2 macrophages.

533 The immunologic and non-immunologic roles of B7-H3 have been previously reported (39).
534 In this study, the difference in tumor growth between the control and B7-H3 KO tumors observed in
535 immunocompetent mice was not observed in immunodeficient mice, suggesting that immunologic
536 effects have a greater influence on tumor growth than non-immunologic effects. B7-H3 has been
537 reported to exert direct immunomodulatory effects mainly on T cells (15,20) and NK cells (40).
538 However, the results of our tumor inoculation experiments in immunodeficient nude mice with
539 normal NK cell function suggest that the effect of B7-H3 on NK cells is not significant.

540 We confirmed both the direct and indirect immunosuppressive effects of B7-H3 on T cells.
541 The increased number of IFN γ ⁺CD8⁺ T cells in B7-H3 KO tumors and B7-H3-low HGSOE cases, both
542 of which were not accompanied by changes in the number of CD8⁺ T cells, suggests that B7-H3 is not
543 involved in the recruitment of T cells; instead, it attenuates T-cell activity at the tumor site either
544 directly or indirectly through M2 macrophages. Several studies have reported T cell-suppressive
545 functions for M2 macrophages (41,42). Although it remains unclear which between the direct and
546 indirect effects contribute more to T-cell suppression, the fact that CCR2 blocking *in vivo* decreased
547 the number of M2 macrophages and increased that of IFN γ ⁺CD8⁺ T cells and inhibited tumor growth
548 indicates that the M2 macrophage-mediated indirect effects significantly affect tumor growth.

549 In tumor tissues, B7-H3 is expressed not only in tumor cells but also in other stromal cells
550 (16,20). Although B7-H3 expression in antigen-presenting cells has been reported to regulate T-cell
551 function (15,19), its role in other normal cells in tumor tissues remains to be elucidated. Our results

552 showed that B7-H3 expression in stromal cells does not significantly affect tumor growth. This result
553 is similar to that reported by a study on MC38 mouse colon cancer cells, in which no difference in
554 tumor growth was observed in the presence or absence of stromal B7-H3 (16). By contrast, another
555 study on E.G7-OVA mouse lymphoma cells showed delayed tumor growth in the absence of stromal
556 B7-H3 (43). These contrasting results suggest that the effect of stromal B7-H3 expression on tumor
557 growth may vary depending on tumor type.

558 To date, the B7-H3 receptor remains unknown, and it is unclear how B7-H3 acts among cells
559 or within B7-H3-expressing cells. The spontaneous dimerization of B7-H3 *in vitro* suggests that
560 B7-H3 among neighboring cells may transmit signals to each other (44). IL20RA has been identified
561 as a binding partner of B7-H3 (45). The involvement of B7-H3 in the activation of intracellular
562 signals, such as STAT3 in tumor cells, has also been revealed (21-23). We found decreased nuclear
563 phosphorylated STAT3 following B7-H3 suppression and CCL2 downregulation by STAT3 inhibitors
564 in tumor cells. These findings indicate that B7-H3 partly acts via STAT3–CCL2 intracellular
565 signaling in the cancer cells expressing B7-H3 or among neighboring cancer cells. Further
566 elucidation of the molecular mechanism underlying B7-H3-mediated signaling, including the
567 identification of its receptors, is thus required.

568 In TCGA-OV, we found that B7-H3 expression negatively correlated with an IFN γ signature
569 and PD-L1 expression. Non-immunoreactive, B7-H3-high, and PD-L1-low HGSOc tumors are not
570 expected to benefit from ICI treatment, and therefore, require a different treatment strategy than
571 that used for immunoreactive tumors. M2 macrophages promote tumor progression in ovarian
572 cancer (46,47), and the abundance of M2 macrophages is an important distinctive characteristic of
573 cancer subtypes with poor prognosis (48,49). We found a positive correlation between B7-H3
574 expression and the number of M2 macrophages in HGSOc cases. CCR2 inhibition had no
575 therapeutic effect on B7-H3-suppressed tumors with sparse M2 macrophages, whereas in
576 B7-H3-expressing tumors with abundant M2 macrophages, it exerted a mild therapeutic effect,
577 suggesting that M2 macrophages are potential therapeutic targets in patients with B7-H3-high, M2
578 macrophage-rich tumors. Ongoing clinical trials targeting macrophages are expected to be effective
579 in such tumor subtypes (50). Our findings also confirm those of a previous study which stated that
580 anti-B7-H3 treatment reduces immature myeloid cells, including macrophages (32), suggesting that
581 B7-H3 suppression could be effective in reducing the number of M2 macrophages. In addition to its
582 previously reported clinical applications, including as a direct inhibitor of T cells and a pan-tumor
583 antigen with high selectivity, B7-H3 may be a promising therapeutic target in cancers with a M2
584 macrophage-mediated immunosuppressive TME.

585 There are several limitations to this study. We did not identify the upstream regulators of
586 B7-H3 expression, and hence the fundamental causes that shape the differential immunological
587 TME. B7-H3 upregulation in tumor cells was not observed by the addition of any cytokines,
588 including IFN γ in our *in vitro* experiments. The relationship between B7-H3 expression and genetic
589 factors, such as tumor mutation burden (TMB), remains unknown. Verhaak et al. report that the

590 differentiated type has lower TMB and aneuploidy than other subtypes, whereas the proliferative
591 type has fewer germline *BRCA* 1/2 mutations than other subtypes (10). Desbois et al. found no
592 differences in TMB or *BRCA* mutations, homologous recombination deficiency (HRD) status, or
593 microsatellite instability (MSI) status among the molecular subtypes of HGSOC (14). Therefore, it
594 remains unclear when and how B7-H3 expression and the immunoreactive TME are determined.
595 The identification of the definitive drivers is warranted in future studies.

596 In conclusion, we revealed the involvement of B7-H3 in the CCL2–CCR2–M2 macrophage
597 axis and in the immunosuppressive TME in HGSOC. Our findings further the understanding of the
598 immunological TME and demonstrate the promising potential of B7-H3 as a therapeutic target for
599 the B7-H3-high, M2 macrophage-rich, unfavorable phenotype of HGSOC.

600

601 **Acknowledgements**

602 This work was supported by the Grants-in-Aid for Strategic Medical Science Research (grant
603 numbers 18K16769 and 20K18210) from the Ministry of Education, Culture, Sports, Science, and
604 Technology of Japan. We would like to thank Editage (www.editage.com) for English language
605 editing.

606 **References**

- 607 1. Sung H, Ferlay J, Siegel RL, Laversanne M, Soerjomataram I, Jemal A, *et al.* Global cancer
608 statistics 2020: GLOBOCAN estimates of incidence and mortality worldwide for 36 cancers in
609 185 countries. *CA Cancer J Clin* 2021. doi 10.3322/caac.21660.
- 610 2. Ray-Coquard I, Pautier P, Pignata S, Perol D, Gonzalez-Martin A, Berger R, *et al.* Olaparib
611 plus bevacizumab as first-line maintenance in ovarian cancer. *N Engl J Med*
612 2019;**381**(25):2416–28. doi 10.1056/NEJMoa1911361.
- 613 3. Gonzalez-Martin A, Pothuri B, Vergote I, DePont Christensen R, Graybill W, Mirza MR, *et al.*
614 Niraparib in patients with newly diagnosed advanced ovarian cancer. *N Engl J Med*
615 2019;**381**(25):2391–402. doi 10.1056/NEJMoa1910962.
- 616 4. Matulonis UA, Shapira-Frommer R, Santin AD, Lisysanskaya AS, Pignata S, Vergote I, *et al.*
617 Antitumor activity and safety of pembrolizumab in patients with advanced recurrent ovarian
618 cancer: results from the phase II KEYNOTE-100 study. *Ann Oncol* 2019;**30**(7):1080–7. doi
619 10.1093/annonc/mdz135.
- 620 5. Moore KN, Bookman M, Sehouli J, Miller A, Anderson C, Scambia G, *et al.* LBA31 primary
621 results from IMagyn050/GOG 3015/ENGOT-OV39, a double-blind placebo (pbo)-controlled
622 randomised phase III trial of bevacizumab (bev)-containing therapy +/- atezolizumab (atezo)
623 for newly diagnosed stage III/IV ovarian cancer (OC). *Ann Oncol* 2020;**31**:S1161-S2. doi
624 10.1016/j.annonc.2020.08.2261.
- 625 6. Disis ML, Taylor MH, Kelly K, Beck JT, Gordon M, Moore KM, *et al.* Efficacy and safety of
626 avelumab for patients with recurrent or refractory ovarian cancer: phase 1b results from the
627 JAVELIN solid tumor trial. *JAMA Oncol* 2019;**5**(3):393–401. doi
628 10.1001/jamaoncol.2018.6258.
- 629 7. Izar B, Tirosh I, Stover EH, Wakiro I, Cuoco MS, Alter I, *et al.* A single-cell landscape of
630 high-grade serous ovarian cancer. *Nat Med* 2020;**26**(8):1271–9. doi
631 10.1038/s41591-020-0926-0.
- 632 8. Armstrong DK, Alvarez RD, Bakkum-Gamez JN, Barroilhet L, Behbakht K, Berchuck A, *et al.*
633 Ovarian cancer, Version 2.2020, NCCN Clinical Practice Guidelines in Oncology. *J Natl*
634 *Compr Canc Netw* 2021;**19**(2):191–226. doi 10.6004/jncn.2021.0007.
- 635 9. Cancer Genome Atlas Research N. Integrated genomic analyses of ovarian carcinoma. *Nature*
636 2011;**474**(7353):609–15. doi 10.1038/nature10166.
- 637 10. Verhaak RG, Tamayo P, Yang JY, Hubbard D, Zhang H, Creighton CJ, *et al.* Prognostically
638 relevant gene signatures of high-grade serous ovarian carcinoma. *J Clin Invest*
639 2013;**123**(1):517–25. doi 10.1172/JCI65833.
- 640 11. Chin CD, Fares CM, Campos M, Chen HW, Shintaku IP, Konecny GE, *et al.* Association of
641 PD-L1 expression by immunohistochemistry and gene microarray with molecular subtypes of
642 ovarian tumors. *Mod Pathol* 2020;**33**(10):2001–10. doi 10.1038/s41379-020-0567-3.
- 643 12. Mandai M, Hamanishi J, Abiko K, Matsumura N, Baba T, Konishi I. Dual faces of

- 644 IFN γ in cancer progression: A role of PD-L1 induction in the determination of pro- and
645 antitumor immunity. *Clin Cancer Res* 2016;**22**(10):2329–34. doi
646 10.1158/1078-0432.CCR-16-0224.
- 647 13. Taki M, Abiko K, Baba T, Hamanishi J, Yamaguchi K, Murakami R, *et al.* Snail promotes
648 ovarian cancer progression by recruiting myeloid-derived suppressor cells via CXCR2 ligand
649 upregulation. *Nat Commun* 2018;**9**(1):1685. doi 10.1038/s41467-018-03966-7.
- 650 14. Desbois M, Udyavar AR, Ryner L, Kozlowski C, Guan Y, Durrbaum M, *et al.* Integrated
651 digital pathology and transcriptome analysis identifies molecular mediators of T-cell
652 exclusion in ovarian cancer. *Nat Commun* 2020;**11**(1):5583. doi 10.1038/s41467-020-19408-2.
- 653 15. Chapoval AI, Ni J, Lau JS, Wilcox RA, Flies DB, Liu D, *et al.* B7-H3: A costimulatory
654 molecule for T cell activation and IFN- γ production. *Nat Immunol* 2001;**2**(3):269–74.
655 doi 10.1038/85339.
- 656 16. Seaman S, Zhu Z, Saha S, Zhang XM, Yang MY, Hilton MB, *et al.* Eradication of tumors
657 through simultaneous ablation of CD276/B7-H3-positive tumor cells and tumor vasculature.
658 *Cancer Cell* 2017;**31**(4):501–15 e8. doi 10.1016/j.ccell.2017.03.005.
- 659 17. Modak S, Zanzonico P, Grkovski M, Slotkin EK, Carrasquillo JA, Lyashchenko SK, *et al.*
660 B7H3-directed intraperitoneal radioimmunotherapy with radioiodinated omburtamab for
661 desmoplastic small round cell tumor and other peritoneal tumors: Results of a phase I study.
662 *J Clin Oncol* 2020;**38**(36):4283–91. doi 10.1200/JCO.20.01974.
- 663 18. Du H, Hirabayashi K, Ahn S, Kren NP, Montgomery SA, Wang X, *et al.* Antitumor Responses
664 in the Absence of Toxicity in Solid Tumors by Targeting B7-H3 via Chimeric Antigen Receptor
665 T cells. *Cancer Cell* 2019;**35**(2):221–37 e8. doi 10.1016/j.ccell.2019.01.002.
- 666 19. Prasad DV, Nguyen T, Li Z, Yang Y, Duong J, Wang Y, *et al.* Murine B7-H3 is a negative
667 regulator of T cells. *J Immunol* 2004;**173**(4):2500–6. doi 10.4049/jimmunol.173.4.2500.
- 668 20. Hofmeyer KA, Ray A, Zang X. The contrasting role of B7-H3. *Proc Natl Acad Sci U S A*
669 2008;**105**(30):10277–8. doi 10.1073/pnas.0805458105.
- 670 21. Liu H, Tekle C, Chen YW, Kristian A, Zhao Y, Zhou M, *et al.* B7-H3 silencing increases
671 paclitaxel sensitivity by abrogating Jak2/Stat3 phosphorylation. *Mol Cancer Ther*
672 2011;**10**(6):960–71. doi 10.1158/1535-7163.MCT-11-0072.
- 673 22. Tekle C, Nygren MK, Chen YW, Dybsjord I, Nesland JM, Maelandsmo GM, *et al.* B7-H3
674 contributes to the metastatic capacity of melanoma cells by modulation of known
675 metastasis-associated genes. *Int J Cancer* 2012;**130**(10):2282–90. doi 10.1002/ijc.26238.
- 676 23. Lin L, Cao L, Liu Y, Wang K, Zhang X, Qin X, *et al.* B7-H3 promotes multiple myeloma cell
677 survival and proliferation by ROS-dependent activation of Src/STAT3 and c-Cbl-mediated
678 degradation of SOCS3. *Leukemia* 2019;**33**(6):1475–86. doi 10.1038/s41375-018-0331-6.
- 679 24. Murakami R, Matsumura N, Mandai M, Yoshihara K, Tanabe H, Nakai H, *et al.*
680 Establishment of a Novel Histopathological Classification of High-Grade Serous Ovarian
681 Carcinoma Correlated with Prognostically Distinct Gene Expression Subtypes. *Am J Pathol*

- 682 2016;**186**(5):1103–13. doi 10.1016/j.ajpath.2015.12.029.
- 683 25. Broberg P. Statistical methods for ranking differentially expressed genes. *Genome Biol*
684 2003;**4**(6):R41. doi 10.1186/gb-2003-4-6-r41.
- 685 26. Barbie DA, Tamayo P, Boehm JS, Kim SY, Moody SE, Dunn IF, *et al.* Systematic RNA
686 interference reveals that oncogenic KRAS-driven cancers require TBK1. *Nature*
687 2009;**462**(7269):108–12. doi 10.1038/nature08460.
- 688 27. Ayers M, Lunceford J, Nebozhyn M, Murphy E, Loboda A, Kaufman DR, *et al.*
689 IFN-gamma-related mRNA profile predicts clinical response to PD-1 blockade. *J Clin Invest*
690 2017;**127**(8):2930–40. doi 10.1172/JCI91190.
- 691 28. Abiko K, Mandai M, Hamanishi J, Yoshioka Y, Matsumura N, Baba T, *et al.* PD-L1 on tumor
692 cells is induced in ascites and promotes peritoneal dissemination of ovarian cancer through
693 CTL dysfunction. *Clin Cancer Res* 2013;**19**(6):1363–74. doi 10.1158/1078-0432.CCR-12-2199.
- 694 29. Hox V, O'Connell MP, Lyons JJ, Sackstein P, Dimaggio T, Jones N, *et al.* Diminution of signal
695 transducer and activator of transcription 3 signaling inhibits vascular permeability and
696 anaphylaxis. *J Allergy Clin Immunol* 2016;**138**(1):187–99. doi 10.1016/j.jaci.2015.11.024.
- 697 30. Schust J, Sperl B, Hollis A, Mayer TU, Berg T. Stattic: A small-molecule inhibitor of STAT3
698 activation and dimerization. *Chem Biol* 2006;**13**(11):1235–42. doi
699 10.1016/j.chembiol.2006.09.018.
- 700 31. Hamanishi J, Mandai M, Iwasaki M, Okazaki T, Tanaka Y, Yamaguchi K, *et al.* Programmed
701 cell death 1 ligand 1 and tumorinfiltrating CD8 T lymphocytes are prognostic factors of
702 human ovarian cancer. *Proc Natl Acad Sci U S A* 2007;**104**(9):3360–5. doi
703 10.1073/pnas.0611533104.
- 704 32. Mao L, Fan TF, Wu L, Yu GT, Deng WW, Chen L, *et al.* Selective blockade of B7-H3 enhances
705 antitumour immune activity by reducing immature myeloid cells in head and neck squamous
706 cell carcinoma. *J Cell Mol Med* 2017;**21**(9):2199–210. doi 10.1111/jcmm.13143.
- 707 33. Lee C, Jeong H, Bae Y, Shin K, Kang S, Kim H, *et al.* Targeting of M2-like tumor-associated
708 macrophages with a melittin-based pro-apoptotic peptide. *J Immunother Cancer*
709 2019;**7**(1):147. doi 10.1186/s40425-019-0610-4.
- 710 34. Mulati K, Hamanishi J, Matsumura N, Chamoto K, Mise N, Abiko K, *et al.* VISTA expressed
711 in tumour cells regulates T cell function. *Br J Cancer* 2019;**120**(1):115–27. doi
712 10.1038/s41416-018-0313-5.
- 713 35. Peng J, Hamanishi J, Matsumura N, Abiko K, Murat K, Baba T, *et al.* Chemotherapy induces
714 programmed cell death-ligand 1 overexpression via the nuclear factor-kappaB to foster an
715 immunosuppressive tumor microenvironment in ovarian cancer. *Cancer Res*
716 2015;**75**(23):5034–45. doi 10.1158/0008-5472.CAN-14-3098.
- 717 36. Wang R, Ma Y, Zhan S, Zhang G, Cao L, Zhang X, *et al.* B7-H3 promotes colorectal cancer
718 angiogenesis through activating the NF-kappaB pathway to induce VEGFA expression. *Cell*
719 *Death Dis* 2020;**11**(1):55. doi 10.1038/s41419-020-2252-3.

- 720 37. Kang FB, Wang L, Li D, Zhang YG, Sun DX. Hepatocellular carcinomas promote
721 tumor-associated macrophage M2-polarization via increased B7-H3 expression. *Oncol Rep*
722 2015;**33**(1):274-82. doi 10.3892/or.2014.3587.
- 723 38. Mao Y, Chen L, Wang F, Zhu D, Ge X, Hua D, *et al.* Cancer cell-expressed B7-H3 regulates
724 the differentiation of tumor-associated macrophages in human colorectal carcinoma. *Oncol*
725 *Lett* 2017;**14**(5):6177-83. doi 10.3892/ol.2017.6935.
- 726 39. Kontos F, Michelakos T, Kurokawa T, Sadagopan A, Schwab JH, Ferrone CR, *et al.* B7-H3: An
727 Attractive Target for Antibody-based Immunotherapy. *Clin Cancer Res* 2021;**27**(5):1227-35.
728 doi 10.1158/1078-0432.CCR-20-2584.
- 729 40. Castriconi R, Dondero A, Augugliaro R, Cantoni C, Carnemolla B, Sementa AR, *et al.*
730 Identification of 4Ig-B7-H3 as a neuroblastoma-associated molecule that exerts a protective
731 role from an NK cell-mediated lysis. *Proc Natl Acad Sci U S A* 2004;**101**(34):12640-5. doi
732 10.1073/pnas.0405025101.
- 733 41. Van de Velde LA, Subramanian C, Smith AM, Barron L, Qualls JE, Neale G, *et al.* T cells
734 encountering myeloid cells programmed for amino acid-dependent immunosuppression use
735 rictor/mTORC2 protein for proliferative checkpoint decisions. *J Biol Chem* 2017;**292**(1):15-30.
736 doi 10.1074/jbc.M116.766238.
- 737 42. Benner B, Scarberry L, Suarez-Kelly LP, Duggan MC, Campbell AR, Smith E, *et al.*
738 Generation of monocyte-derived tumor-associated macrophages using tumor-conditioned
739 media provides a novel method to study tumor-associated macrophages in vitro. *J*
740 *Immunother Cancer* 2019;**7**(1):140. doi 10.1186/s40425-019-0622-0.
- 741 43. Lee YH, Martin-Orozco N, Zheng P, Li J, Zhang P, Tan H, *et al.* Inhibition of the B7-H3
742 immune checkpoint limits tumor growth by enhancing cytotoxic lymphocyte function. *Cell*
743 *Res* 2017;**27**(8):1034-45. doi 10.1038/cr.2017.90.
- 744 44. Vigdorovich V, Ramagopal UA, Lazar-Molnar E, Sylvestre E, Lee JS, Hofmeyer KA, *et al.*
745 Structure and T cell inhibition properties of B7 family member, B7-H3. *Structure*
746 2013;**21**(5):707-17. doi 10.1016/j.str.2013.03.003.
- 747 45. Husain B, Ramani SR, Chiang E, Lehoux I, Paduchuri S, Arena TA, *et al.* A platform for
748 extracellular interactome discovery identifies novel functional binding partners for the
749 immune receptors B7-H3/CD276 and PVR/CD155. *Mol Cell Proteomics* 2019;**18**(11):2310-23.
750 doi 10.1074/mcp.TIR119.001433.
- 751 46. Hensler M, Kasikova L, Fiser K, Rakova J, Skapa P, Laco J, *et al.* M2-like macrophages
752 dictate clinically relevant immunosuppression in metastatic ovarian cancer. *J Immunother*
753 *Cancer* 2020;**8**(2):e000979. doi 10.1136/jitc-2020-000979.
- 754 47. Maccio A, Gramignano G, Cherchi MC, Tanca L, Melis L, Madeddu C. Role of M1-polarized
755 tumor-associated macrophages in the prognosis of advanced ovarian cancer patients. *Sci Rep*
756 2020;**10**(1):6096. doi 10.1038/s41598-020-63276-1.
- 757 48. Tekpli X, Lien T, Rossevold AH, Nebdal D, Borgen E, Ohnstad HO, *et al.* An independent

- 758 poor-prognosis subtype of breast cancer defined by a distinct tumor immune
759 microenvironment. *Nat Commun* 2019;**10**(1):5499. doi 10.1038/s41467-019-13329-5.
- 760 49. Wang Q, Hu B, Hu X, Kim H, Squatrito M, Scarpace L, *et al*. Tumor Evolution of
761 Glioma-Intrinsic Gene Expression Subtypes Associates with Immunological Changes in the
762 Microenvironment. *Cancer Cell* 2017;**32**(1):42–56 e6. doi 10.1016/j.ccell.2017.06.003.
- 763 50. DeNardo DG, Ruffell B. Macrophages as regulators of tumour immunity and immunotherapy.
764 *Nat Rev Immunol* 2019;**19**(6):369–82. doi 10.1038/s41577-019-0127-6.

765 **Figure legends**

766 **Figure 1. *CD276* (B7-H3) expression is upregulated in the non-immunoreactive tumor**
767 **microenvironment of HGSOc.** **a**, Microarray analysis of HGSOc clinical samples from Kyoto
768 University ($n=30$). The immunoreactive ($n=8$) and non-immunoreactive ($n=22$) subtypes were
769 compared using the Samroc method. The magenta dot represents *CD276* (B7-H3). **b**, *CD276*
770 expression among the molecular subtypes of 263 HGSOc samples from TCGA-OV. Data are
771 presented as the mean \pm SEM; ** $P<0.01$, *** $P<0.001$, N.S.: not significant by one-way ANOVA with
772 Tukey's multiple comparison test. **c**, Gene expression comparison of T cell-suppressive B7 family
773 molecules in the immunoreactive and non-immunoreactive subtypes of TCGA-OV. Data are
774 presented as the mean \pm SEM after Z-score normalization. *** $P<0.001$ by one-way ANOVA. **d**,
775 Pearson's correlation analysis of the IFN γ signature activity scores and expression of T
776 cell-suppressive B7 family molecules in TCGA-OV. Values after Z-score normalization are plotted.
777 * $P<0.05$, *** $P<0.001$. (Green and blue dots represent the immunoreactive and non-immunoreactive
778 subtypes, respectively, in **b-d**.

779

780 **Figure 2. B7-H3 contributes to tumor progression via an immune-related mechanism in murine**
781 **ovarian cancer models.** **a**, Flow cytometry of B7-H3 knockout (KO) HM-1 and ID8 and their
782 respective controls. Blue, pink, and gray histograms represent B7-H3 KO cells, B7-H3 control cells,
783 and the isotype control, respectively. **b**, Representative B7-H3 IHC (top) and immunofluorescence
784 (bottom) images of controls and HM-1 B7-H3 KO tumors for the indicated markers. α SMA-positive
785 fibroblasts represented by black and white arrowheads. Scale bar, 50 μ m. Positive cells were stained
786 brown in IHC, and red (α SMA), green (B7-H3), and blue (DAPI) in immunofluorescence images. **c**,
787 Intradermal tumor volume (left, $n=6$) and omental tumor weight at day 10 (right, $n=6$) of
788 immunocompetent mice injected with HM-1 B7-H3 KO or control cells. **d**, Changes in body weight
789 (top, $n=5-6$) and omental tumor weight at day 52 (bottom, $n=6$) of immunocompetent mice
790 intraperitoneally injected with ID8 B7-H3 KO or control cells. **e**, Intradermal tumor volume (left,
791 $n=5$) and omental tumor weight at day 10 (right, $n=6$) of immunodeficient mice injected with HM-1
792 B7-H3 KO or control cells. **f**, Changes in body weight (top, $n=6$) and omental tumor weight at day 52
793 (bottom, $n=6$) of immunodeficient mice intraperitoneally injected with ID8 B7-H3 KO or control cells.
794 **c-f**, Data are presented as the mean \pm SEM; *** $P<0.001$, N.S.: not significant, unpaired t -test.

795

796 **Figure 3. B7-H3 suppression in tumor cells decreases the number of intratumoral M2 macrophage**
797 **and increases IFN γ production of CD8 $^+$ T cells.** **a**, IHC of CD206 in the B7-H3 KO intradermal HM-1
798 tumors and the controls ($n=3$). CD206 $^+$ cells were stained brown. Scale bar, 50 μ m. **b**, Flow cytometry
799 of mice from **a**. Density plots (upper left) show the M2 macrophages at day 12. Each dot represents
800 live CD45 $^+$ cells, and the boxed area represents F4/80 $^+$ CD206 $^+$ M2 macrophages. The percentage of
801 positive cells relative to the total cells is plotted ($n=6$). **c**, Quantitative PCR for the indicated genes in
802 F4/80 $^+$ macrophages (M ϕ) isolated from the HM-1 intradermal tumors ($n=5$). **d**, T-cell proliferation in

803 presence of HM-1 tumor-derived macrophages. Upper histograms show the percentage of
804 proliferating T cells co-cultured (4:1) with macrophages from control or B7-H3 KO tumors. Lower bar
805 graph shows the percentage of proliferating T cells co-cultured with various ratios of macrophages
806 ($n=5$). **e**, IFN γ levels in the supernatants of co-cultures in **d** ($n=5$). **f**, Flow cytometry of IFN γ ⁺CD8⁺ T
807 cells from HM-1 tumors. Each dot represents live CD45⁺CD3⁺ cells, and the boxed area represents
808 IFN γ ⁺CD8⁺ T cells. The percentage of IFN γ ⁺CD8⁺ T cells relative to total CD8⁺ T cells is plotted ($n=6$).
809 **a-f**, Data are presented as the mean \pm SEM; * $P<0.05$, ** $P<0.01$, *** $P<0.001$, N.S.: not significant,
810 unpaired t -test.

811

812 **Figure 4. B7-H3 suppression downregulates CCL2 production, in part, via the STAT3 pathway in**
813 **ovarian cancer cells.** **a**, Differential gene expression based on RNA-sequencing between controls
814 ($n=3$) and B7-H3 KO ($n=3$) groups in HM-1 and ID8 cells and HM-1 intradermal tumors. **b, c**, CCL2
815 protein in the (b) culture supernatants and (c) tumors derived from HM-1 B7-H3 KO (top), ID8
816 B7-H3 KO (bottom), and their respective controls ($n=5$).

817 **d**, CCL2 protein in the culture supernatants of the OVCAR3 shB7-H3 (top), OVCA420 shB7-H3
818 (bottom), and their respective controls ($n=5$). **e, f**, Representative Western blot of nuclear
819 phosphorylated-STAT3 (p-STAT3) in (e) HM-1 and ID8 and (f) OVCAR3 and OVCA420 cells. Lower
820 bar graphs show the signal intensity of p-STAT3 relative to the TBP control in HM-1 and ID8 (both
821 $n=10$) and OVCAR3 and OVCA420 cells (both $n=7$). **g, h**, Quantitative PCR for expression of (g) *Ccl2*
822 in HM-1 and ID8 cells and (h) *CCL2* in OVCAR3 and OVCA420 cells treated with 1.25 and 5 μ M of
823 the STAT3 inhibitors (g) C188-9 and (h) Stattic, respectively. DMSO was used as the control ($n=3$).
824 Data are presented as the mean \pm SEM; * $P<0.05$, ** $P<0.01$, *** $P<0.001$, unpaired t -test in **b, c, e, f**
825 and one-way ANOVA with Tukey's multiple comparisons test in **d, g, h**.

826

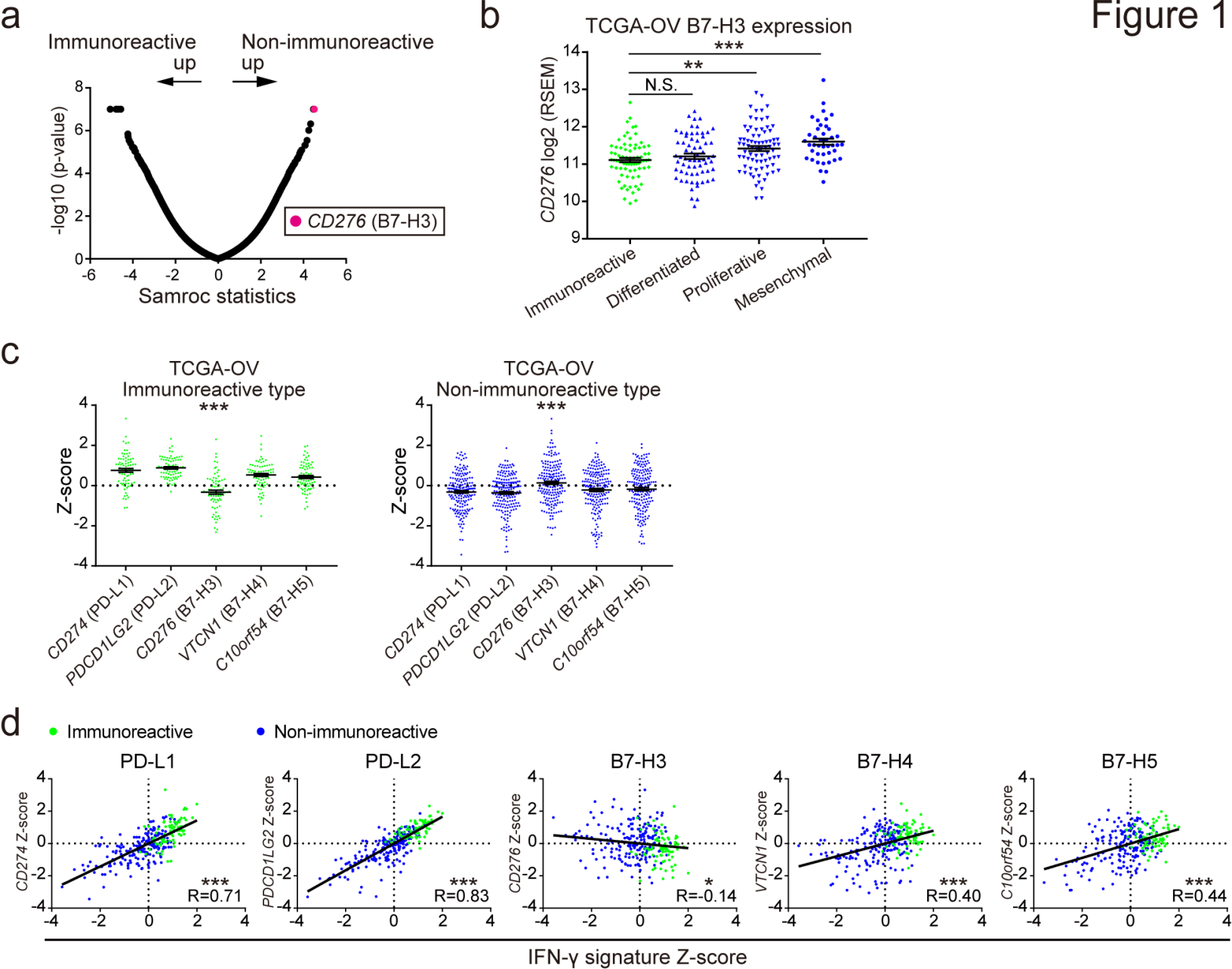
827 **Figure 5. The CCL2–CCR2–M2 macrophage axis contributes to B7-H3-mediated tumor progression.**
828 **a**, Chemotaxis of mouse monocytes (left) and generated M2 macrophages (right) in response to HM-1
829 control or B7-H3 KO tumor cell-conditioned medium (TCM). Monocytes or M2 macrophages were
830 pretreated with 2 μ M RS504393 (CCR2 antagonist) or DMSO before plating. MEM-Alpha was used
831 as the negative control ($n=3$). **b**, Differentiation of mouse monocytes into M2 macrophages in
832 response to HM-1 control or B7-H3 KO TCM supplemented with 20 μ g/mL anti-CCL2 or control IgG.
833 MEM-Alpha was used as the negative control ($n=3$). **c**, Tumor growth in mice intradermally injected
834 with HM-1 B7-H3 KO cells or control cells and treated with RS504393 (2 mg/kg body weight) or
835 DMSO daily following tumor inoculation. **d**, Flow cytometric analysis of the treated tumors in **c** ($n=6$).
836 Data are presented as the mean \pm SEM (* $P < 0.05$, ** $P < 0.01$, *** $P < 0.001$, N.S.: not significant,
837 one-way ANOVA with Tukey's multiple comparisons test in **a, b**, and unpaired t -test in **c, d**).

838

839 **Figure 6. B7-H3 expression associates with an M2 macrophage-rich, IFN γ ⁺CD8 T cell-poor TME and**
840 **a poor prognosis in HGSOC patients.** **a**, Correlation between CCL2 expression and B7-H3 protein in

841 primary HGSOc tumors ($n=28$) analyzed by Spearman's correlation analysis. **b**, Representative
842 images of HGSOc samples showing B7-H3 expression and CD206⁺, CD8⁺, and IFN γ ⁺CD8⁺ cells.
843 Cells were stained with hematoxylin and eosin or immunostained with the corresponding antibodies.
844 Scale bar, 100 μ m. Positive cells were stained brown in IHC, and red (CD8), green (IFN γ), and blue
845 (DAPI) in immunofluorescence slides. The boxed area represents the zoomed image shown in the
846 upper right corner. **c**, Correlation between the infiltration of CD206⁺ cells and B7-H3 expression in
847 the corresponding primary tumors of HGSOc ($n=62$) analyzed using Jonckheere-Terpstra test. Data
848 are presented as the median with 95 % confidence intervals. **d**, Correlation between
849 tumor-infiltrating CD8⁺ and IFN γ ⁺CD8⁺ T cells ($n=62$) analyzed using Spearman's correlation
850 analysis. Blue and pink dots represent B7-H3-low and -high expression cases, respectively. **e**,
851 Comparisons of the number of tumor-infiltrating CD8⁺ T cells (left) and IFN γ ⁺CD8⁺ T cells (right) in
852 B7-H3-low and -high expression groups by immunostaining ($n=62$). Data are presented as the
853 median with 95 % confidence intervals; * $P<0.05$, N.S.: not significant, Mann-Whitney's U test. **f**,
854 Progression-free survival (left) and overall survival (right) of patients with HGSOc ($n=62$). Patients
855 were classified into a B7-H3-low group ($n=31$) and B7-H3-high group ($n=31$). * $P<0.05$, log-rank test.

Figure 1



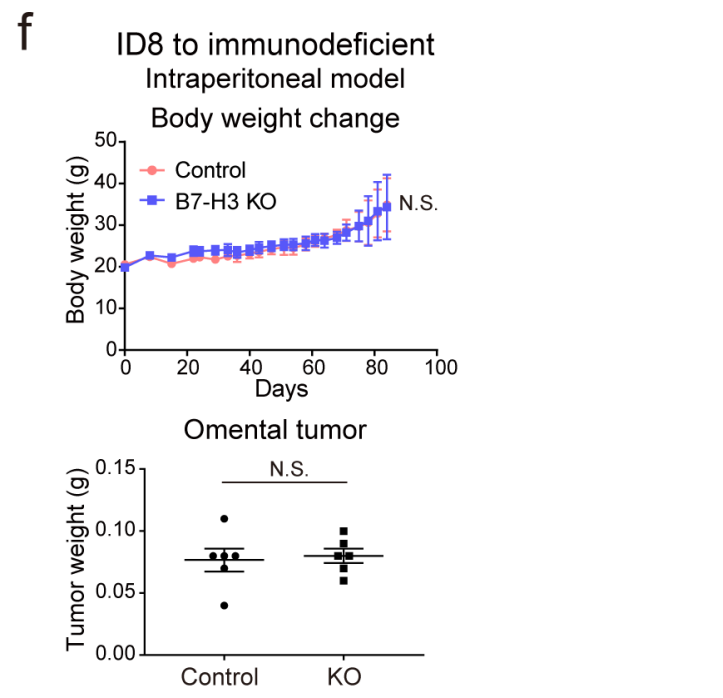
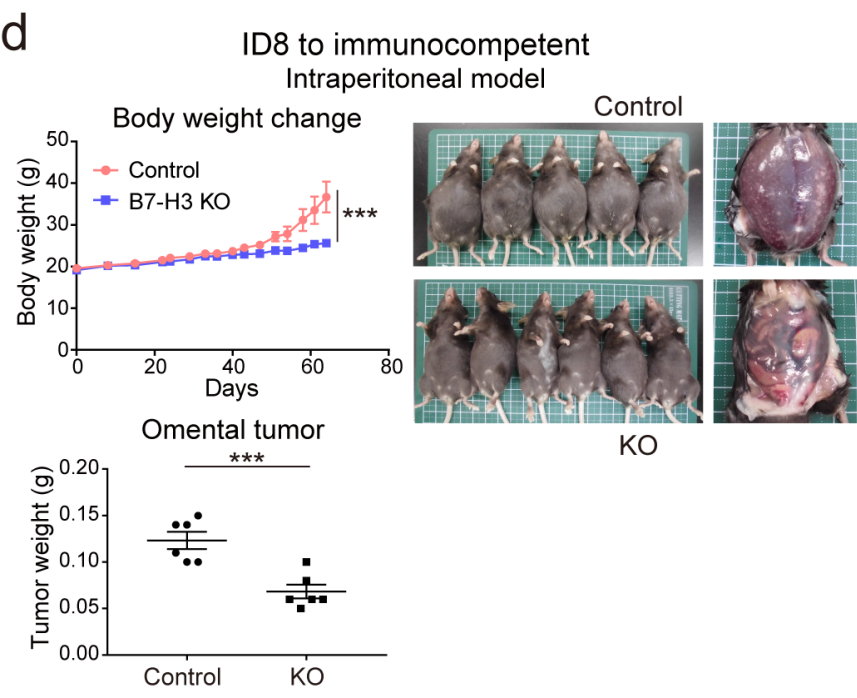
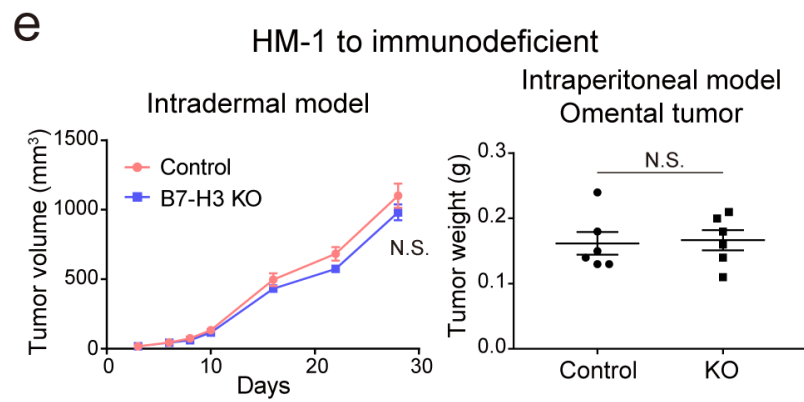
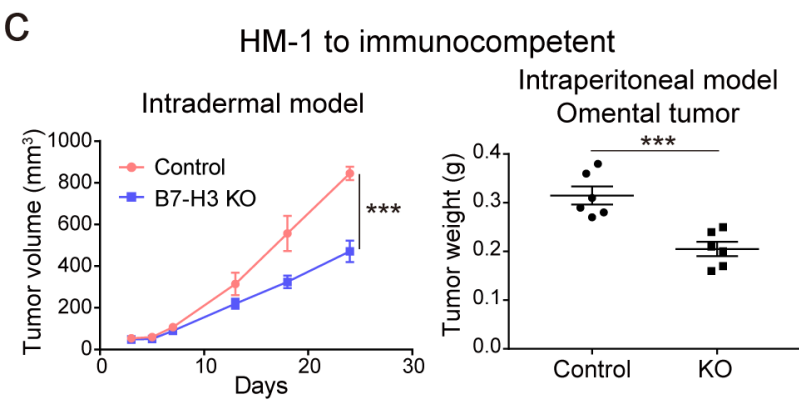
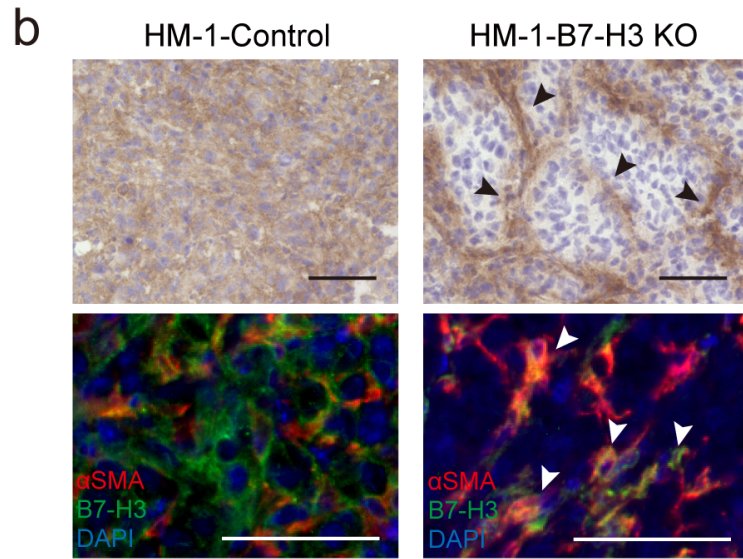
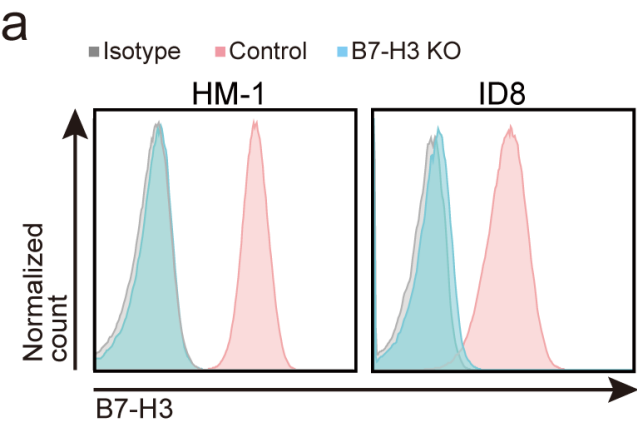


Figure 3

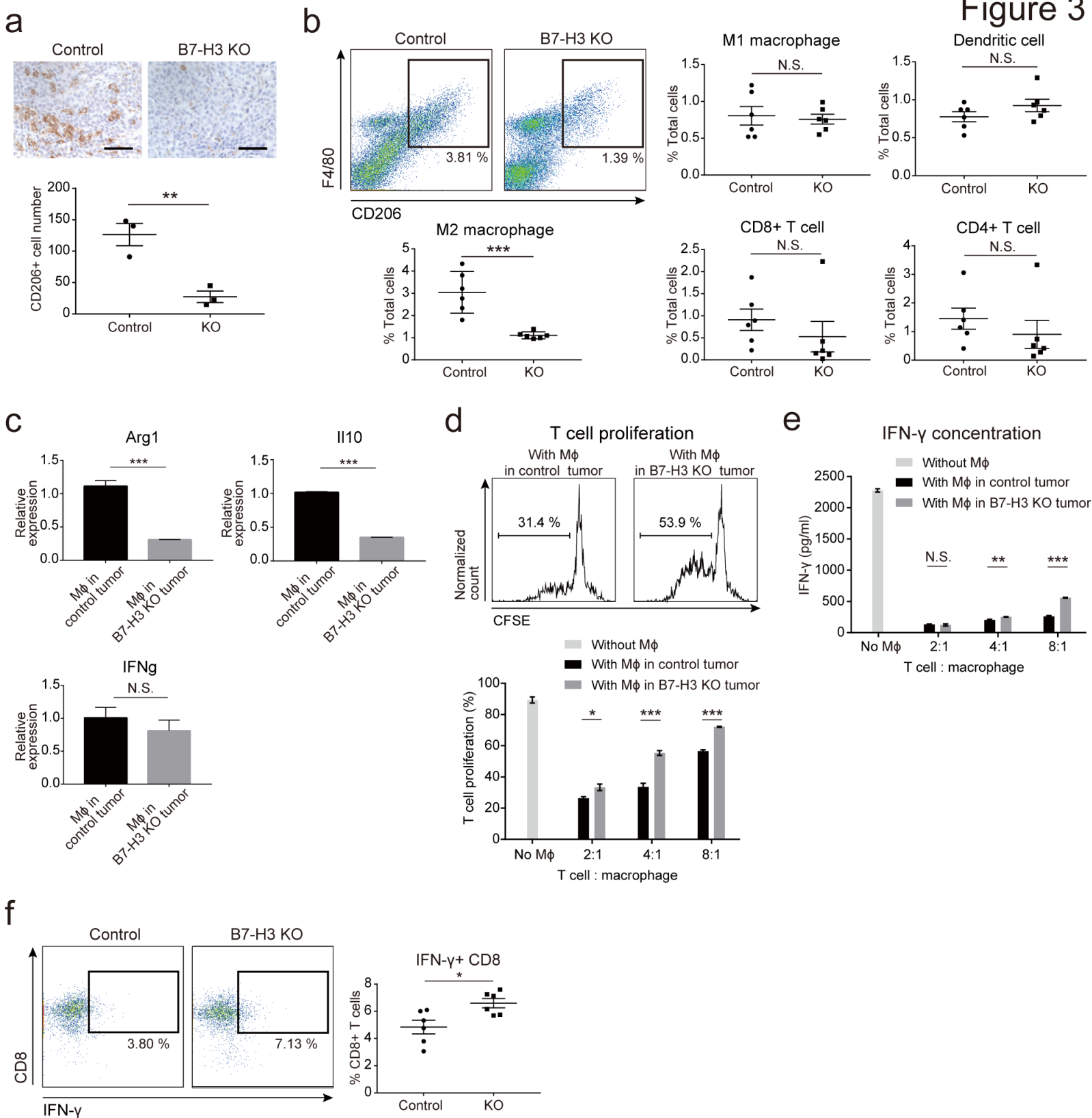


Figure 4

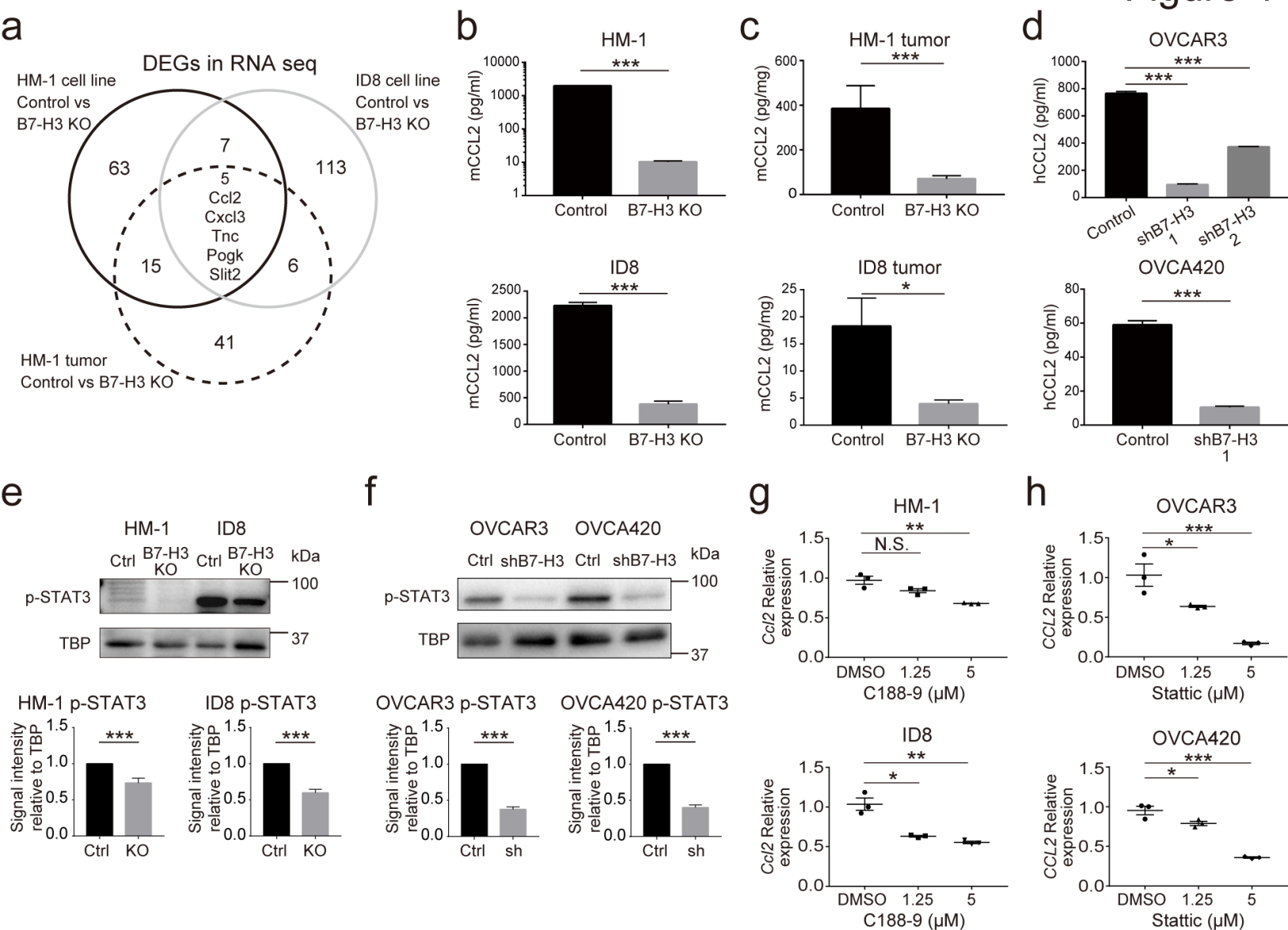


Figure 5

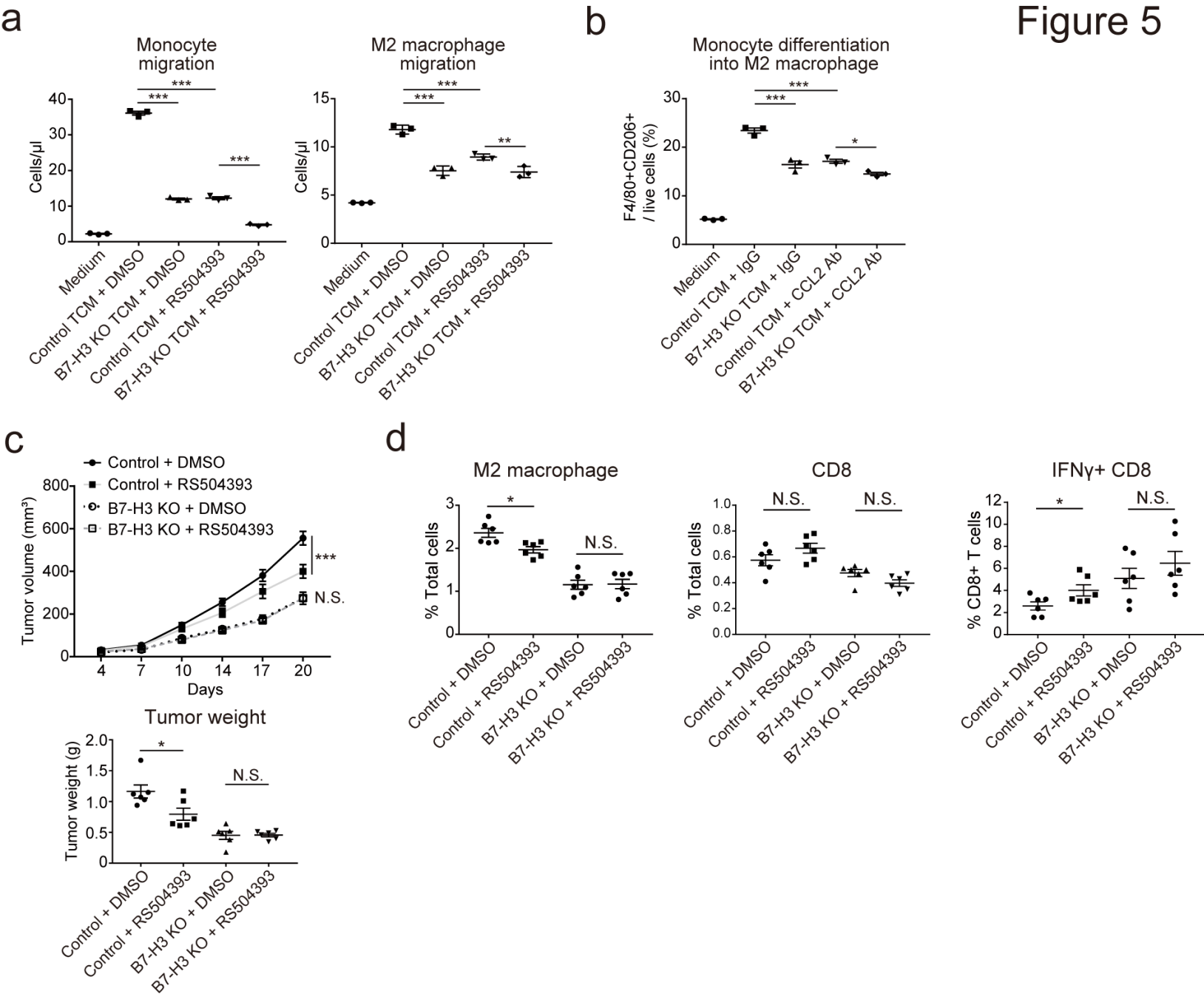
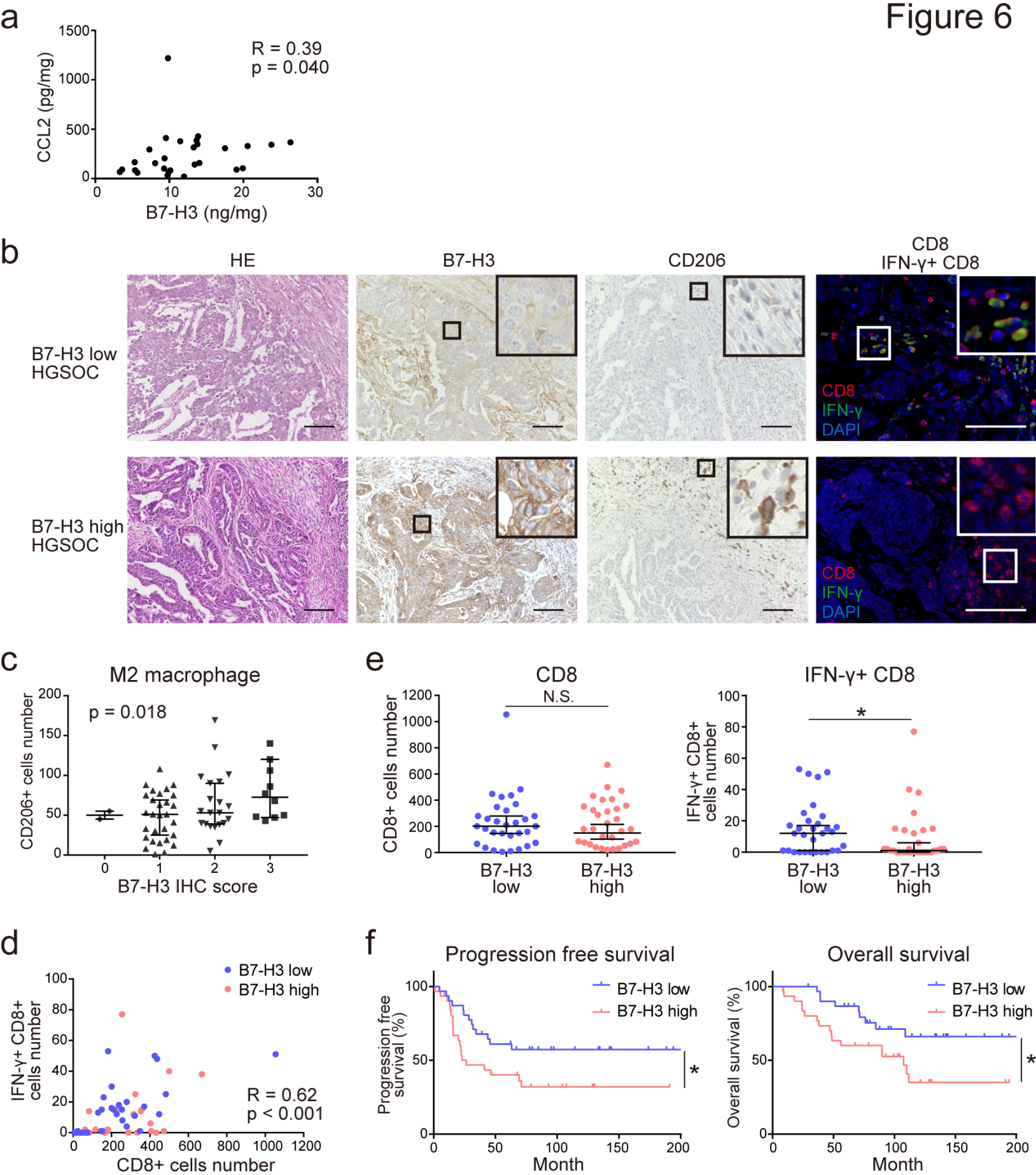


Figure 6



Cancer Immunology Research

B7-H3 suppresses anti-tumor immunity via the CCL2-CCR2-M2 macrophage axis and contributes to ovarian cancer progression

Taito Miyamoto, Ryusuke Murakami, Junzo Hamanishi, et al.

Cancer Immunol Res Published OnlineFirst November 19, 2021.

Updated version	Access the most recent version of this article at: doi: 10.1158/2326-6066.CIR-21-0407
Supplementary Material	Access the most recent supplemental material at: http://cancerimmunolres.aacrjournals.org/content/suppl/2021/11/20/2326-6066.CIR-21-0407.DC1
Author Manuscript	Author manuscripts have been peer reviewed and accepted for publication but have not yet been edited.

E-mail alerts	Sign up to receive free email-alerts related to this article or journal.
Reprints and Subscriptions	To order reprints of this article or to subscribe to the journal, contact the AACR Publications Department at pubs@aacr.org .
Permissions	To request permission to re-use all or part of this article, use this link http://cancerimmunolres.aacrjournals.org/content/early/2021/11/19/2326-6066.CIR-21-0407 . Click on "Request Permissions" which will take you to the Copyright Clearance Center's (CCC) Rightslink site.